New York Journal of Mathematics

New York J. Math. **21** (2015) 547–599.

Dynamics of the monodromies of the fibrations on the magic 3-manifold

Eiko Kin

Abstract. We study the magic manifold N which is a hyperbolic and fibered 3-manifold. We give an explicit construction of a fiber F_a and its monodromy : $F_a \to F_a$ of the fibration associated to each fibered class a of N. Let δ_g (resp. δ_g^+) be the minimal dilatation of pseudo-Anosovs (resp. pseudo-Anosovs with orientable invariant foliations) defined on an orientable closed surface of genus g. As a consequence of our result, we obtain the first explicit construction of the following pseudo-Anosovs; a minimizer of δ_7^+ and conjectural minimizers of δ_g for large g.

Contents

1. Introduction

In this paper, we explore the dynamics of monodromies of fibrations on a hyperbolic, fibered 3-manifold, called the *magic* 3*-manifold* N, which is the exterior of the 3 chain link $\mathcal{C}_3$, see Figure 1(1). We first set some notations, then describe the motivation of our study. Let Σ be an orientable surface (possibly with punctures). A homeomorphism $\Phi : \Sigma \to \Sigma$ is *pseudo-Anosov* if there exist a pair of transverse measured foliations $(\mathcal{F}^u, \mu^u)$ and $(\mathcal{F}^s, \mu^s)$ and a constant $\lambda = \lambda(\Phi) > 1$ such that

$$\Phi(\mathcal{F}^u, \mu^u) = (\mathcal{F}^u, \lambda\mu^u) \quad \text{and} \quad \Phi(\mathcal{F}^s, \mu^s) = (\mathcal{F}^s, \lambda^{-1}\mu^s).$$

Then $\mathcal{F}^u$ and $\mathcal{F}^s$ are called the *unstable* and *stable foliations* (or *invariant foliations*), and λ is called the *dilatation* of Φ. Let $\mathrm{Mod}(\Sigma)$ be the mapping

Received October 7, 2014.

2010 *Mathematics Subject Classification.* Primary 57M27, 37E30, Secondary 37B40.

Key words and phrases. Pseudo-Anosov, dilatation, topological entropy, train track representative, magic manifold, branched surface.

The author is supported by Grant-in-Aid for Scientific Research (C) (No. 15K04875), Japan Society for the Promotion of Science.

ISSN 1076-9803/2015

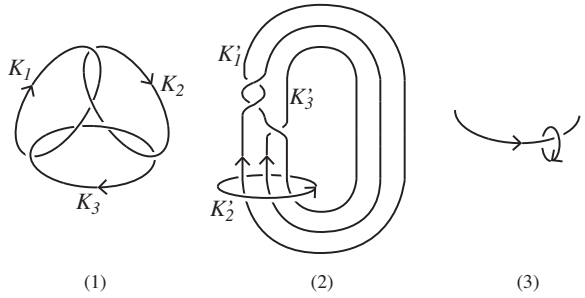

FIGURE 1. (1) 3 chain link $\mathcal{C}_3$. (2) Braided link $\mathrm{br}(\sigma_1^2\sigma_2^{-1})$. Our convention of the orientation is that the meridian of a component of the link is chosen as in (3).

class group of Σ, that is $\mathrm{Mod}(\Sigma)$ is the group of isotopy classes of orientation preserving homeomorphisms on Σ fixing punctures setwise. A mapping class $\phi \in \mathrm{Mod}(\Sigma)$ is called *pseudo-Anosov* if ϕ contains a pseudo-Anosov homeomorphism $\Phi : \Sigma \to \Sigma$ as a representative. The topological entropy $\mathrm{ent}(\Phi)$ of Φ is equal to $\log \lambda(\Phi)$, and $\mathrm{ent}(\Phi)$ attains the minimal entropy among all homeomorphisms which are isotopic to Φ, see [5, Exposé 10]. In the case $\phi = [\Phi]$, we denote by $\lambda(\phi)$ and $\mathrm{ent}(\phi)$, the dilatation $\lambda(\Phi)$ and topological entropy $\mathrm{ent}(\Phi) = \log \lambda(\Phi)$.

We take an element $\phi \in \mathrm{Mod}(\Sigma)$. Let $\mathbb{T}_\phi$ be its mapping torus, i.e., if Φ is a representative of ϕ, then

$$\mathbb{T}_\phi = \Sigma \times \mathbb{R}/\sim$$

where $\sim$ identifies $(x, t+1)$ with $(\Phi(x), t)$ for $x \in \Sigma$ and $t \in \mathbb{R}$. Such a Φ is called the *monodromy* of $\mathbb{T}_\phi$. The vector field $\frac{\partial}{\partial t}$ on $\Sigma \times \mathbb{R}$ induces a flow Φ^t on $\mathbb{T}_\phi$, which is called the *suspension flow*. The hyperbolization theorem by Thurston [36] tells us that a 3-manifold M which is homeomorphic to $\mathbb{T}_\phi$ admits a hyperbolic structure if and only if ϕ is pseudo-Anosov. The magic manifold N is in fact a hyperbolic, fibered 3-manifold, since N is homeomorphic to a 4-puncture sphere bundle over the circle with the pseudo-Anosov monodromy as in Figure 1(2) (see Lemma 2.6(1)).

In a paper [35] Thurston introduced a norm $\|\cdot\|$ on $H_2(M, \partial M; \mathbb{R})$ for hyperbolic 3-manifolds and proved that the unit ball U_M with respect to the Thurston norm $\|\cdot\|$ is a compact, convex polyhedron. When M is homeomorphic to a hyperbolic, fibered 3-manifold $\mathbb{T}_\phi$, he gave a connection between the Thurston norm $\|\cdot\|$ and fibrations on M. In particular if such a 3-manifold M has the second Betti number $b_2(M)$ which is greater than 1, he proved that there exists a top dimensional face Ω on ∂U_M, called a *fibered face* such that every integral class a of $H_2(M, \partial M; \mathbb{Z})$ which is in the open cone over Ω corresponds to a fiber F_a of the fibration associated to a with a monodromy $\Phi_a : F_a \to F_a$, that is $\mathbb{T}_{\phi_a}$ is homeomorphic to M, where $\phi_a = [\Phi_a]$. Such an integral class a is called a *fibered class*.

Since $\phi_a = [\Phi_a]$ is pseudo-Anosov for each fibered class a, M provides infinitely many pseudo-Anosovs on fibers with distinct topological types. A theorem by Fried [6, 7] asserts that the monodromy $\Phi_a : F_a \to F_a$ and the (un)stable foliation $\mathcal{F}_a$ of Φ_a can be described by using the suspension flow Φ^t and the suspension of the (un)stable foliation of Φ. We pose the question: how describe practical constructions of $\Phi_a : F_a \to F_a$ and $\mathcal{F}_a$ for each fibered class a? The theorem by Fried does not give us concrete descriptions of them.

E. Hironaka gave concrete descriptions of the monodromies of fibrations associated to sequences of fibered classes on some class of hyperbolic fibered 3-manifolds, see [11, 12]. However no one constructed explicitly the monodromy of the fibration associated to *all* of the fibered classes on a single hyperbolic, fibered 3-manifold M with $b_2(M) > 1$. In this paper we describe them concretely for the magic manifold N. The motivation of our study comes from minimal dilatations on pseudo-Anosovs and their asymptotic behaviors. We fix a surface Σ, and consider the set of dilatations of pseudo-Anosovs on Σ,

$$\mathrm{dil}(\Sigma) = \{\lambda(\phi) \mid \phi \in \mathrm{Mod}(\Sigma) \text{ is pseudo-Anosov}\}.$$

Arnoux–Yoccoz and Ivanov observed that for any constant $c > 1$, there exist finite elements $\lambda \in \mathrm{dil}(\Sigma)$ so that $\lambda < c$, see [15]. In particular, there exists a minimum $\delta(\Sigma)$ of $\mathrm{dil}(\Sigma)$. Let Σ_g be a closed surface of genus g, and $\Sigma_{g,n}$ a closed surface of genus g removing $n \geq 1$ punctures. We let $\delta_g = \delta(\Sigma_g)$ and $\delta_{g,n} = \delta(\Sigma_{g,n})$. We denote by D_n, an n-punctured disk. A mapping class $\phi \in \mathrm{Mod}(D_n)$ defines a mapping class $\phi' \in \mathrm{Mod}(\Sigma_{0,n+1})$ fixing a puncture and vice versa. Moreover ϕ is pseudo-Anosov if and only if ϕ' is pseudo-Anosov. In this case the equality $\lambda(\phi) = \lambda(\phi')$ holds. Thus $\delta(D_n)$ is equal to the minimal dilatation of pseudo-Anosov elements $\phi' \in \mathrm{Mod}(\Sigma_{0,n+1})$ fixing a puncture. In particular we have $\delta(D_n) \geq \delta(\Sigma_{0,n+1})$.

The minimal dilatation problem is to determine an explicit value of $\delta(\Sigma)$, and to identify a pseudo-Anosov element $\phi \in \mathrm{Mod}(\Sigma)$ which achieves $\delta(\Sigma)$ (i.e., minimizer of $\delta(\Sigma)$). A naive but natural question is this: What does a pseudo-Anosov homeomorphism Φ on Σ which achieves $\delta(\Sigma)$ look like? In other words, what does a train track representative of $\phi = [\Phi]$ (which enables us to describe the dynamics of $\Phi : \Sigma \to \Sigma$) look like?

Some of the minimal dilatations are already determined. Also there are partial results. For example, δ_2 is computed in [4], but an explicit value of δ_g is not known for $g \geq 3$. If we denote by δ_g^+, the minimal dilatation of pseudo-Anosovs defined on Σ_g with orientable invariant foliations, then explicit values of δ_g^+ for $2 \leq g \leq 8$ except $g = 6$ are known, see [39, 21] and [10, 1, 20]. The minimal dilatation on an n-punctured disk, $\delta(D_n)$ is determined for $3 \leq n \leq 8$, see [34, 9, 22].

The asymptotic behaviors of the minimal dilatations are shown in the left column of Table 1. Here $A_g \asymp B_g$ means that there exists a constant

TABLE 1. Asymptotic behaviors of minimal dilatations and smallest known upper bounds, where $\delta(D_4) \approx 2.2966$ is the largest root of $t^4 - 2t^3 - 2t + 1$ [34], and $\delta(D_5) \approx 1.7220$ is the largest root of $t^4 - t^3 - t^2 - t + 1$ [9].

asymptotic behaviors	smallest known upper bounds
$\log \delta_g \asymp 1/g$ [33]	(U1) $\limsup_{g\to\infty} g \log \delta_g \le \log(\frac{3+\sqrt{5}}{2})$ [10, 1, 20]
$\log \delta_g^+ \asymp 1/g$ [29, 14]	(U2) $\limsup_{\substack{g\not\equiv 0 \pmod 6 \\ g\to\infty}} g \log \delta_g^+ \le \log(\frac{3+\sqrt{5}}{2})$ [10, 17] (U3) $\limsup_{\substack{g\equiv 6 \pmod{12} \\ g\to\infty}} g \log \delta_g^+ \le 2 \log \delta(D_5)$ [17]
$\log \delta_{0,n} \asymp 1/n$ [14]	(U4) $\limsup_{n\to\infty} n \log \delta_{0,n} \le 2\log(2+\sqrt{3})$ [14, 18]
$\log \delta_{1,n} \asymp 1/n$ [37]	(U5) $\limsup_{n\to\infty} n \log \delta_{1,n} \le 2 \log \delta(D_4)$ [17]
Given $g \ge 2$, $\log \delta_{g,n} \asymp \frac{\log n}{n}$ [37]	(U6) $\limsup_{n\to\infty} \frac{n \log \delta_{g,n}}{\log n} \le 2$ if g enjoys $(*)$ [19]

$c > 0$ which does not depend on g so that $\frac{A_g}{c} < B_g < cA_g$. As we can see from table, we have $\log \delta_{0,n} \asymp 1/n$ and $\log \delta_{1,n} \asymp 1/n$, but a result by Tsai [37] says that the situation in the case $g \ge 2$ is quite different from the case $g = 0$ or 1. In the right column of Table 1, the smallest known upper bounds of the minimal dilatation. We give a precise condition $(*)$ in (U6) in the following.

Theorem 1.1 ([19])**.** *Suppose that $g \ge 2$ satisfies*

$(*)$ $\gcd(2g+1, s) = 1$ *or* $\gcd(2g+1, s+1) = 1$ *for each* $0 \le s \le g$.

Then

$$\limsup_{n\to\infty} \frac{n \log \delta_{g,n}}{\log n} \le 2. \tag{1.1}$$

In particular, if $2g+1$ is prime, then g enjoys $(*)$, and hence (1.1) *holds.*

The upper bounds (U1)–(U6) are realized by sequences of monodromies of the magic manifold N after possibly Dehn filling cusps along the boundary slopes of the fibrations. This is also true for known minimizers of the minimal dilatations δ_2, $\delta(D_n)$ for $3 \le n \le 8$ and δ_g^+ for $2 \le g \le 8$ except $g = 6$. For (U1)–(U5), the sequences project to a single fibered face, and the image of each sequence converges to some interior point. For (U6), the sequence also projects to a single fibered face, and the image converges to a point on the boundary of the fibered face. These results say that the topological types of fibers of fibrations on N are surprisingly full of variety. However, no explicit constructions of sequences of pseudo-Anosovs needed for the proofs of (U1)–(U6) except (U4) were given so far. Also an explicit example of a minimizer of δ_7^+ was not given. In this paper we prove the following which allows us to construct pseudo-Anosovs in question explicitly.

Theorem 1.2. *We have algorithms to construct the following. For each fibered class a of N:*

(1) *the monodromy $\Phi_a : F_a \to F_a$ of the fibration on N associated to a,*
(2) *in the case a is primitive, a train track representative $\mathfrak{p}_a : \tau_a \to \tau_a$ of $\phi_a = [\Phi_a]$ whose incidence matrix is Perron–Frobenius.*

In [30] Oertel constructs branched surfaces which carry fibers of fibrations on hyperbolic, fibered 3-manifolds. In the proof of Theroem 1.2(1), we construct branched surfaces $\mathcal{B}_+$ and $\mathcal{B}_-$ following [30] which carry fibers of fibrations associated to fibered classes on N.

It is well-known that a train track representative $\mathfrak{p}_a : \tau_a \to \tau_a$ as in Theorem 1.2(2) can recover a pseudo-Anosov homeomorphism which represents ϕ_a, and it serves the monodromy $\Phi_a : F_a \to F_a$ of the fibration associated to a. However we do not need the claim (2) for the proof of (1). We can construct the both fiber F_a and monodromy $\Phi_a : F_a \to F_a$ in an explicit and combinatorial way.

Let $N(r)$ be the manifold obtained from N by Dehn filling one cusp along the slope $r \in \mathbb{Q}$. See Figure 1(3) for our convention of the orientation. As a consequence of Theorem 1.2, we can give constructive descriptions of monodromies of fibrations associated to any fibered class on the hyperbolic, fibered manifolds $N(r)$ for infinitely many $r \in \mathbb{Q}$. For example, we can do them for Whitehead sister link exterior $N(\frac{3}{-2})$, the simplest 3-braided link exterior $N(\frac{1}{-2})$ and the Whitehead link exterior $N(1)$. In particular, we can construct the following pseudo-Anosov homeomorphisms explicitly:

- A minimizer of δ_7^+, see Example 4.3.
- Conjectural minimizers of δ_g^+ for $g \equiv 2, 4 \pmod 6$, see [21, Question 6.1]. See also Remark 1.3 and Example 4.2.
- Conjectural minimizers of δ_g^+ for large g such that $g \not\equiv 0 \pmod 6$, see [17, Conjecture 1.12(2)]. See also Examples 4.2, 4.3, 4.4.
- Conjectural minimizer of δ_g for large g, see [17, Conjecture 1.12(1)]. See also Example 4.3.
- Conjectural minimizers of $\delta_{1,n}$ for large n, see [17, Conjecture 1.13]. See also Example 4.5.
- Sequences of pseudo-Anosov homeomorphisms to give the smallest known upper bounds (U1)–(U6) in Table 1.

Remark 1.3. Hironaka gave the first explicit construction of the orientable train track representative on Σ_g for $g \equiv 2, 4 \pmod 6$ whose dilatation equals the conjectural minimum δ_g^+ for such a g, see [13]. Hironaka also constructed explicitly the infinite subsequence of pseudo-Anosov homeomorphisms defined on Σ_g with some condition on g to prove the upper bounds (U1) and (U2), see [11].

Problem 1.4. Find the word which represents the mapping class $\phi_a = [\Phi_a]$ for each fibered class a of N by using the standard generating set on

$\mathrm{Mod}(\Sigma_{g,n})$. Its word length could be long, but it would be represented by a simple word, see Remark 3.11.

Problem 1.5. Develop the methods given in Section 3 and prove the same claim in Theorem 1.2 for some class of hyperbolic, fibered 3-manifolds.

The paper is organized as follows. In Section 2, we review basic facts on train tracks, the Thurston norm and clique polynomials. We also review some properties of the magic manifold. In Section 3, we prove Theorem 1.2. In the proof, we construct the directed graph Γ_a with a metric on the set of edges, which is induced from the train track representative $\mathfrak{p}_a : \tau_a \to \tau_a$ of ϕ_a. Such a directed graph Γ_a captures the dynamics of both $\Phi_a : F_a \to F_a$ and $\mathfrak{p}_a : \tau_a \to \tau_a$. Then we construct the curve complex G_a induced from Γ_a, which is an undirected, weighted graph on the set of vertices. Such curve complexes are studied by McMullen [28]. In our setting, G_a gives us some insight into what the train track representative $\mathfrak{p}_a : \tau_a \to \tau_a$ looks like. In Section 4, we exhibit some subsequences of pseudo-Anosovs which can be used in the proof of the upper bounds (U1)–(U6). We find that the types of curve complexes in each subsequence are fixed. These curve complexes give us some hints to know what the pseudo-Anosovs with the smallest dilations look like.

Acknowledgements. The author thanks Hideki Miyachi, Mitsuhiko Takasawa and Hiroyuki Minakawa. H. Miyachi and M. Takasawa gave valuable comments on this paper. H. Minakawa gave a series of lectures on his work at Osaka University in 2004. The author learned many things on pseudo-Anosovs and pseudo-Anosov flows during his course. Theorem 1.2(1) is inspired by his construction of pseudo-Anosovs [29].

2. Preliminaries

2.1. Train tracks. Definitions and basic results on train tracks are contained in [32]. See also [24]. In this section, we recall them for the convenience of the readers.

Throughout the paper, surfaces are orientable. Let F be a surface with possibly punctures or boundary. Let τ be a branched 1-submanifold on F. We say that τ is a *train track* if:

(1) τ is a smooth graph such that the edges are tangent at the vertices, i.e., τ looks as in Figure 2(1) near each vertex of τ.
(2) Each component of $F \setminus \tau$ is a disk with more than 3 cusps on its boundary or an annulus with more than 1 cusp on one boundary component and with no cusps on the other boundary component (i.e., the other boundary component is the one of ∂F or a puncture of F).

See Figure 9(1) for an example of a train track on $\Sigma_{0,4}$.

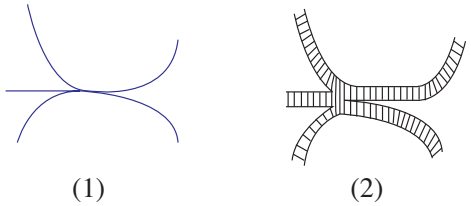

FIGURE 2. (1) Train track near vertex. (2) Fibered neighborhood.

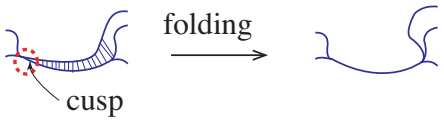

FIGURE 3. Folding map near a cusp.

Two edges of τ which are tangent at some vertex make a *cusp*, see Figure 3(left). Associated to the train track τ, we can define a fibered neighborhood $\mathcal{N}(\tau) \subset F$ whose fibers are segments given by a retraction $\mathcal{N}(\tau) \searrow \tau$. The fibers in this case are called *ties*, see Figure 2(2).

Let $\mathcal{F}$ be a measured foliation on F. We say that $\mathcal{F}$ *is carried by* τ if $\mathcal{F}$ can be represented by a partial measured foliation whose support is $\mathcal{N}(\tau)$ and which is transverse to the ties. (For the definition of partial measured foliations, see [32, Section 1.2].)

Let σ be a train track on F. We say that σ *is carried by* τ if σ is isotopic to a train track σ' which is contained in $\mathcal{N}(\tau)$ and which is transverse to the ties (said differently, every smooth edge path on σ' is transverse to the ties). Let $f : F \to F$ be a homeomorphism. A train track τ is *invariant under* $[f]$ if $f(\tau)$ is carried by τ, that is, $f(\tau)$ is isotopic to some train track σ' which satisfies the above. In this case, folding edges of τ' near cusps repeatedly (see Figure 3 for a folding map), in other words, (up to isotopy) collapsing τ' onto τ smoothly yields a map $\mathfrak{p} : \tau \to \tau$ such that $\mathfrak{p}$ maps vertices to vertices, and $\mathfrak{p}$ is locally injective at any points which do not map into vertices. Such a $\mathfrak{p} : \tau \to \tau$ is called a *train track representative* of $[f]$. An edge e of τ is said to be *infinitesimal* (for $\mathfrak{p}$) if e is eventually periodic under $\mathfrak{p}$, that is $\mathfrak{p}^{m+n}(e) = \mathfrak{p}^n(e)$ for integers $m > 0$ and $n \geq 0$. Other edges of τ are said to be *real*. Let k be the number of the real edges of τ. Then we have a $k \times k$ nonnegative integer matrix $M_{\mathfrak{p}} = (m_{ij})$, called the *incidence matrix* or *transition matrix* for $\mathfrak{p} : \tau \to \tau$ *(with respect to real edges)*, where m_{ij} is the number of times so that the image $\mathfrak{p}(e_j)$ of the jth real edge passes through the ith real edge e_i in either direction. Also, $\mathfrak{p} : \tau \to \tau$ determines a finite, directed graph $\Gamma_{\mathfrak{p}}$ by taking a vertex for each real edge of τ, and then adding m_{ij} directed edges from the jth real edge e_j to the ith real edge e_i. In other words, we have m_{ij} directed edges from e_j to e_i if $\mathfrak{p}(e_j)$ passes through e_i in

either direction m_{ij} times . We say that $\Gamma_{\mathfrak{p}}$ is the *induced directed graph* of $\mathfrak{p} : \tau \to \tau$.

A square, nonnegative integer matrix M is said to be *Perron–Frobenius* if there exists an integer $\ell \geq 1$ such M^ℓ is positive, that is each entry of M^ℓ is positive. In this case, the spectral radius of M is given by the largest eigenvalue of M called the *Perron–Frobenius eigenvalue*, see [8].

The following theorem is well known.

Theorem 2.1 (Theorem 4.1 in [32] and its proof.)**.** *If $\Phi : F \to F$ is a pseudo-Anosov homeomorphism, then there exists a train track τ on F which carries the unstable foliation $\mathcal{F}^u$ of Φ and a train track representative $\mathfrak{p} : \tau \to \tau$ of $\phi = [\Phi]$. Such a representative $\mathfrak{p} : \tau \to \tau$ has the property that the incidence matrix $M_{\mathfrak{p}}$ is Perron–Frobenius and its Perron–Frobenius eigenvalue is exactly equal to $\lambda(\Phi)$.*

Conversely, if $f : F \to F$ is a homeomorphism and if $\mathfrak{p} : \tau \to \tau$ is a train track representative of $\phi = [f]$ such that its incidence matrix $M_{\mathfrak{p}}$ is Perron–Frobenius, then ϕ is pseudo-Anosov whose dilatation $\lambda(\phi)$ equals the Perron–Frobenius eigenvalue of $M_{\mathfrak{p}}$, see Bestvina–Handel [2, Section 3.4].

2.2. Thurston norm, fibered face, entropy function. We review the basic results on the Thurston norm and the relation between the Thurston norm and hyperbolic, fibered 3-manifolds developed by Thurston, Fried, Matsumoto and McMullen. Let M be an oriented hyperbolic 3-manifold possibly $\partial M \neq \emptyset$. We recall the Thurston norm $\| \cdot \| : H_2(M, \partial M; \mathbb{R}) \to \mathbb{R}$. For more detail, see [35]. Let $F = F_1 \cup F_2 \cup \cdots \cup F_k$ be a finite union of oriented, connected surfaces. We define $\chi_-(F)$ to be

$$\chi_-(F) = \sum_{i=1}^{k} \max\{0, -\chi(F_i)\}.$$

The Thurston norm $\| \cdot \|$ is defined for an integral class $a \in H_2(M, \partial M; \mathbb{Z})$ by

$$\|a\| = \min_F \{\chi_-(F)\},$$

where the minimum is taken over all oriented surfaces F embedded in M satisfying $a = [F]$. The surface F which realizes the minimum is called a *minimal representative* of a. Then $\| \cdot \|$ admits a unique continuous extension $\| \cdot \| : H_2(M, \partial M; \mathbb{R}) \to \mathbb{R}$ which is linear on rays through the origin. It is known that the unit ball $U_M \subset H_2(M, \partial M; \mathbb{R})$ with respect to the Thurston norm $\| \cdot \|$ is a finite-sided polyhedron [35].

Let Ω be any top dimensional face on the boundary ∂U_M of the Thurston norm ball. We denote by C_Ω, the cone over Ω with the origin, and we denote by $\mathrm{int}(C_\Omega)$, the interior of C_Ω. Thurston proved in [35] that if M is a surface bundle over the circle and if F is any fiber of the fibration on M, then there exists a top dimensional face Ω on ∂U_M so that $[F]$ is an integral class of $\mathrm{int}(C_\Omega)$. Moreover for any integral class $a \in \mathrm{int}(C_\Omega)$, its

minimal representative F_a becomes a fiber of a fibration on M. Such a face Ω is called a *fibered face* and an integral class $a \in \mathrm{int}(C_\Omega)$ is called a *fibered class*. Thus, if the second Betti number $b_2(M)$ is greater than 1, then a single 3-manifold M provides infinitely many pseudo-Anosovs on surfaces with different topological types.

Let Ω be a fibered face of M. If $a \in \mathrm{int}(C_\Omega)$ is primitive and integral, then the minimal representative F_a is a connected fiber of the fibration associated a. The mapping class $\phi_a = [\Phi_a]$ of the monodromy $\Phi_a : F_a \to F_a$ of its fibration is pseudo-Anosov (since M is hyperbolic). We define the dilatation $\lambda(a)$ and entropy $\mathrm{ent}(a)$ to be the dilatation and entropy of the pseudo-Anosov ϕ_a. The entropy function defined on primitive fibered classes is naturally extended to rational classes by homogeneity, i.e., for a rational number r and a primitive fibered class a, the entropy of ra is defined to be $\mathrm{ent}(ra) = \frac{1}{|r|}\mathrm{ent}(a)$.

Theorem 2.2 ([7, 26, 27])**.** *The function given by $a \mapsto \mathrm{ent}(a)$ for each rational class $a \in \mathrm{int}(C_\Omega)$ extends to a real analytic convex function on $\mathrm{int}(C_\Omega)$. The restriction $\mathrm{ent}|_{\mathrm{int}(\Omega)} : \mathrm{int}(\Omega) \to \mathbb{R}$ is a strictly convex function which goes to ∞ toward the boundary of Ω.*

By properties of $\|\cdot\|$ and ent, we see that the *normalized entropy function*

$$\mathrm{Ent} = \|\cdot\|\mathrm{ent} : \mathrm{int}(C_\Omega) \to \mathbb{R}$$

is constant on each ray in $\mathrm{int}(C_\Omega)$ through the origin.

We choose $\phi = [\Phi] \in \mathrm{Mod}(\Sigma)$, and we consider the mapping torus $\mathbb{T}_\phi$ with the suspension flow Φ^t. Hereafter we fix an orientation of Σ so that its normal direction coincides with the flow direction of Φ^t. For $S \subset \Sigma$, we define $S^t \subset \mathbb{T}_\phi$ to be the image of $S \times \{t\} \subset \Sigma \times \{t\}$ under the projection $p : \Sigma \times \mathbb{R} \to \mathbb{T}_\phi$.

Theorem 2.3 (Theorem 7 and Lemma in [6])**.** *Let $\Phi : F \to F$ be a pseudo-Anosov homeomorphism with stable and unstable foliations $\mathcal{F}^s$ and $\mathcal{F}^u$ on an oriented surface F, and let $\phi = [\Phi]$. Let $\widehat{\mathcal{F}^s}$ and $\widehat{\mathcal{F}^u}$ denote the suspensions of $\mathcal{F}^s$ and $\mathcal{F}^u$ by Φ. If Ω is a fibered face on $\mathbb{T}_\phi$ with $[F] \in \mathrm{int}(C_\Omega)$, then for any minimal representative F_a of any fibered class $a \in \mathrm{int}(C_\Omega)$, we can modify F_a by an isotopy which satisfies the following:*

1. *F_a is transverse to the flow Φ^t, and the first return map : $F_a \to F_a$ is precisely the pseudo-Anosov monodromy $\Phi_a : F_a \to F_a$ of the fibration on $\mathbb{T}_\phi$ associated to a. Moreover F_a is unique up to isotopy along flow lines.*
2. *The stable and unstable foliations of the pseudo-Anosov Φ_a are given by $\widehat{\mathcal{F}^s} \cap F_a$ and $\widehat{\mathcal{F}^u} \cap F_a$.*

Following [29], we introduce *flowbands* in $\mathbb{T}_\phi$.

Definition 2.4. Let J_1 and J_2 be embedded arcs in $\mathbb{T}_\phi$. Suppose that J_1 and J_2 are transverse to Φ^t. We say that J_1 *is connected to* J_2 (*with respect*

to Φ^t) if there exists a positive continuous function $\mathfrak{t} : J_1 \to \mathbb{R}$ such that for any $x \in J_1$, we have:

- $\Phi^{\mathfrak{t}(x)}(x) \in J_2$, $\Phi^t(x) \notin J_2$ for $0 < t < \mathfrak{t}(x)$.
- The map $J_1 \to J_2$ given by $x \mapsto \Phi^{\mathfrak{t}(x)}(x)$ is a homeomorphism.

The *flowband* $[J_1, J_2]$ is defined by

$$[J_1, J_2] = \{\Phi^t(x) \mid x \in J_1,\ 0 \leq t \leq \mathfrak{t}(x)\}.$$

Flowbands are used to build branched surfaces in Section 3.3.

2.3. Clique polynomials. We review some results on clique polynomials, developed by McMullen [28]. As we will see in Section 3.7, clique polynomials are useful to compute dilatations of pseudo-Anosov monodromies of fibrations on fibered 3-manifolds.

Let (Γ, m) be a finite, directed graph Γ with a metric $m : E(\Gamma) \to \mathbb{R}_+$ on the set of edges $E(\Gamma)$. The metric m specifies the length of each edge. Parallel edges and loops are allowed. We sometimes denote (Γ, m) by Γ when m is obvious. The *growth rate* $\lambda(\Gamma, m)$ is defined by

$$\lambda(\Gamma, m) = \lim_{T \to \infty} N_0(T)^{1/T},$$

where $N_0(T)$ is the number of the closed, directed paths in Γ of length $\leq T$.

When $m(e)$ is a positive integer for each $e \in E(\Gamma)$, we can add $m(e) - 1$ new vertices along each edge e to obtain a new directed graph Γ' with the metric $\mathbf{1} : E(\Gamma') \to \mathbb{R}_+$ sending each edge to 1. Then we have

$$\lambda(\Gamma, m) = \lambda(\Gamma', \mathbf{1}).$$

Suppose that ϕ is a pseudo-Anosov mapping class. Let $\mathfrak{p} : \tau \to \tau$ be a train track representative of ϕ given in Theorem 2.1 and let $\Gamma_{\mathfrak{p}}$ be the induced directed graph of $\mathfrak{p} : \tau \to \tau$. Theorem 2.1 implies that $(\Gamma_{\mathfrak{p}}, \mathbf{1})$ satisfies

$$\lambda(\phi) = \lambda(\Gamma_{\mathfrak{p}}, \mathbf{1}). \tag{2.1}$$

Let G be a finite, undirected graph with no loops or parallel edges. Let $w : V(G) \to \mathbb{R}_+$ be a weight on the set of vertices $V(G)$. The subset $K \subset V(G)$ forms a *clique* if they span a complete subgraph. (We allow $K = \emptyset$.) The *clique polynomial* of (G, w) is defined by

$$Q(t) = \sum_K (-1)^{(\sharp K)} t^{w(K)},$$

where $\sharp K$ denotes the cardinality of K, the weight of K is given by $w(K) = \sum_{v \in K} w(v)$, and the sum is over all cliques K's of G. We sometimes denote the weighted, undirected graph (G, w) by G when w is obvious.

McMullen relates the growth rates $\lambda(\Gamma, m)$'s to the clique polynomials via the *curve complexes* of (Γ, m)'s. Let $C \subset E(\Gamma)$ be a collection of edges which form a closed, directed loop. If C never visits the same vertex twice, then C is called a *simple curve*. A *multicurve* is a finite union of simple

curves such that no two simple curves share a vertex. The *curve complex* of (Γ, m) is the undirected graph G together with the weight $w : V(G) \to \mathbb{R}_+$, which is obtained by taking a vertex for each simple curve C of Γ, and then joining the two vertices C_1 and C_2 by an edge when (C_1, C_2) is a multicurve of Γ. Then the metric m on $E(\Gamma)$ induces the weight w on $V(G)$ as follows.

$$w(C) = \sum_{e \in C} m(e).$$

Theorem 2.5 ([28])**.** *Let (G, w) be the curve complex of (Γ, m). Then $\frac{1}{\lambda(\Gamma,m)}$ is equal to the the smallest positive root of the clique polynomial $Q(t)$ of (G, w).*

By (2.1) and Theorem 2.5, we can compute the dilatations of pseudo-Anosovs by using the clique polynomials of curve complexes associated to the pseudo-Anosovs. We do not need to compute the characteristic polynomials of the incidence matrices for the dilatations. This observation is due to Birman [3].

2.4. Fibered classes of the magic manifold N. In this section, we review some properties on N which will be used in the paper. We give orientations of components, K_1, K_2 and K_3 of the 3 chain link $\mathcal{C}_3$ as in Figure 1(1). Each component bounds oriented 2-punctured disks, F_α, F_β and F_γ respectively. We set $\alpha = [F_\alpha]$, $\beta = [F_\beta]$, $\gamma = [F_\gamma] \in H_2(N, \partial N; \mathbb{Z})$. Then $\{\alpha, \beta, \gamma\}$ becomes a basis of $H_2(N, \partial N; \mathbb{Z})$. We denote the class $x\alpha + y\beta + z\gamma \in H_2(N, \partial N)$ by (x, y, z). The Thurston norm ball U_N is the parallelepiped with vertices $\pm\alpha = \pm(1, 0, 0)$, $\pm\beta = \pm(0, 1, 0)$, $\pm\gamma = \pm(0, 0, 1)$ and $\pm\alpha + \beta + \gamma = \pm(1, 1, 1)$ ([35, Example 3]), see Figure 5(1). (Note that the minimal representative of κ is taken to be the 3-punctured sphere, embedded in $S^3 \setminus \mathcal{C}_3$, which contains the point $\infty \in S^3 \setminus \mathcal{C}_3$.)

Let $\mathrm{br}(\sigma_1^2\sigma_2^{-1})$ be the 3 components link in S^3 as in Figure 1(2), i.e., it is the link obtained from the closed 3-braid $\sigma_1^2\sigma_2^{-1}$ together with the braid axis. Then $N = S^3 \setminus C_3$ is homeomorphic to $S^3 \setminus \mathrm{br}(\sigma_1^2\sigma_2^{-1})$, see Lemma 2.6(1). This implies that N is a surface bundle over the circle with a fiber of the 4-punctured sphere. Notice that every top dimensional face of ∂U_N is a fibered face, because of the symmetries of $\mathcal{C}_3$. To study monodromies of fibrations on N, we can pick a particular fibered face, for example the fibered face Δ with vertices $(1, 0, 0)$, $(1, 1, 1)$, $(0, 1, 0)$ and $(0, 0, -1)$, see Figure 5(1). The open face $\mathrm{int}(\Delta)$ is written by

$$\mathrm{int}(\Delta) = \{(x, y, z) \mid x + y - z = 1,\ x > 0,\ y > 0,\ x > z,\ y > z\}. \tag{2.2}$$

The Thurston norm $\|a\|$ of $a = (x, y, z) \in C_\Delta$ is given by $x + y - z$. An integral class $(x, y, z) \in C_\Delta$ is fibered (i.e., an integral class (x, y, z) is in $\mathrm{int}(C_\Delta)$ if and only if x, y and z are integers such that $x > 0$, $y > 0$, $x > z$ and $y > z$, see (2.2).

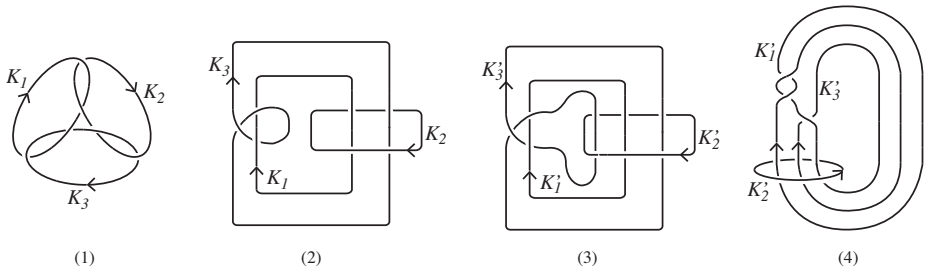

FIGURE 4. (1)(2) 3 chain link $\mathcal{C}_3$, (3)(4) Braided link $\mathrm{br}(\sigma_1^2\sigma_2^{-1})$.

Any class $a = (x, y, z) \in \Delta$ satisfies $z = x + y - 1$. Hence we can write such a class $a = (x, y, z)$ by $[x, y]$. Then we have

$$\mathrm{int}(\Delta) = \{[x, y] \mid 0 < x < 1,\ 0 < y < 1\},$$

see Figure 5(2).

We denote by T_α the torus which is the boundary of a regular neighborhood of K_1. Let $a = (x, y, z) \in \mathrm{int}(C_\Delta)$ be a primitive integral class. We set $\partial_\alpha F_a = \partial F_a \cap T_\alpha$ which consists of the parallel simple closed curves on T_α. We define T_β, $\partial_\beta F_a$ and T_γ, $\partial_\gamma F_a$ in a similar way.

Lemma 2.6 ([18] for (1)(3)(5), [20] for (6)(7), [17] for (4))**.** *Suppose that $a = (x, y, z) \in \mathrm{int}(C_\Delta)$ is a primitive integral class.*

(1) *There is an orientation preserving homeomorphism*

$$: S^3 \setminus \mathcal{C}_3 \to S^3 \setminus \mathrm{br}(\sigma_1^2\sigma_2^{-1})$$

which sends the minimal representative $F_{\alpha+\beta}$ associated to $\alpha + \beta$ to the oriented 3-punctured disk bounded by the braid axis K_2' as in Figure 4(4)*. Thus the pseudo-Anosov homeomorphism which represents the mapping class of $\mathrm{Mod}(\Sigma_{0,4})$ corresponding to $\sigma_1^2\sigma_2^{-1}$ becomes the monodromy $\Phi_{\alpha+\beta} : F_{\alpha+\beta} \to F_{\alpha+\beta}$ of the fibration associated to $\alpha+\beta$.*

(2) *The boundary slope of $\partial_\alpha F_a$ (resp. $\partial_\beta F_a$, $\partial_\gamma F_a$) is given by $\frac{y+z}{-x}$ (resp. $\frac{z+x}{-y}$, $\frac{x+y}{-z}$).*

(3) *We have $\|a\| = x + y - z$. The number of the boundary components of F_a is computed as follows.*

$$\sharp(\partial_\alpha F_a) = \gcd(x, y + z),$$
$$\sharp(\partial_\beta F_a) = \gcd(y, z + x),$$
$$\sharp(\partial_\gamma F_a) = \gcd(z, x + y),$$

where $\gcd(0, w)$ is defined by $|w|$.

(4) *Let $\Phi_{(x,y,z)} : F_{(x,y,z)} \to F_{(x,y,z)}$ be the monodromy of the fibration on N associated to $(x, y, z) \in \mathrm{int}(C_\Delta)$. Then $(y, x, z) \in \mathrm{int}(C_\Delta)$, and $(\Phi_{(x,y,z)})^{-1}$ is conjugate to $\Phi_{(y,x,z)}$.*

(5) *The dilatation* $\lambda(a) = \lambda_{(x,y,z)}$ *is the largest root of*

$$f_{(x,y,z)}(t) = t^{x+y-z} - t^x - t^y - t^{x-z} - t^{y-z} + 1.$$

(6) *The (un)stable foliation* $\mathcal{F}_a$ *of* Φ_a *has a property such that each component of* $\partial_\alpha F_a$, $\partial_\beta F_a$ *and* $\partial_\gamma F_a$ *has* $\frac{x}{\gcd(x,y+z)}$ *prongs,* $\frac{y}{\gcd(y,x+z)}$ *prongs and* $\frac{x+y-2z}{\gcd(z,x+y)}$ *prongs respectively. Moreover* $\mathcal{F}_a$ *does not have singularities in the interior of* F_a.

(7) $\mathcal{F}_a$ *is an orientable foliation if and only if* x *and* y *are even and* z *is odd.*

The proof of (2) is easy. For the convenience of the proof of Lemma 3.4, we prove the claim (1).

Proof of Lemma 2.6(1). First of all, we observe that the link in Figure 4(2) is isotopic to $\mathcal{C}_3$ given in Figure 4(1). Observe also that the link in Figure 4(3) is isotopic to the braided link $\mathrm{br}(\sigma_1^2\sigma_2^{-1})$ given in Figure 4(4). We use the link diagrams in (2) and (3). We cut the twice punctured disk ($\simeq F_\alpha$) bounded by the component K_1. Let F_α^1 and F_α^2 be the resulting twice punctured disks obtained from F_α. We reglue these twice punctured disks twisting either F_α^1 or F_β^2 by 360 degrees. Then we obtain the link in (3) which is isotopic to $\mathrm{br}(\sigma_1^2\sigma_2^{-1})$. This implies that there exists an orientation preserving homeomorphism $h : S^3 \setminus \mathcal{C}_3 \to S^3 \setminus \mathrm{br}(\sigma_1^2\sigma_2^{-1})$. Then one can check that h sends the minimal representative of $\alpha + \beta$ to the desired 3-punctured disk. □

Lemma 2.6(4) allows us to focus on only fibered classes $(x, y, z) \in \mathrm{int}(C_\Delta)$ such that $y \geq x$ for the proof of Theorem 1.2. We now introduce two bases $\{-\gamma, \beta, \alpha + \beta\}$ and $\{\alpha + \beta + \gamma, \beta, \alpha + \beta\}$ of $H_2(N, \partial N, \mathbb{Z})$ to describe such fibered classes (x, y, z). If $z \leq 0$ (resp. $z \geq 0$), then we represent (x, y, z) by the base $\{-\gamma, \beta, \alpha + \beta\}$ (resp. $\{\alpha + \beta + \gamma, \beta, \alpha + \beta\}$). Let us define

$$\begin{aligned}
\Delta_+ &= \{(x, y, z) \in \Delta \mid y \geq x,\ z \geq 0\},\\
\Delta_- &= \{(x, y, z) \in \Delta \mid y \geq x,\ z \leq 0\},\\
\Delta_0 &= \{(x, y, z) \in \Delta \mid y \geq x,\ z = 0\},
\end{aligned}$$

see Figure 5(3)(4), and define $\widehat{\Delta}_\pm \subset \Delta_\pm$ as follows.

$$\begin{aligned}
\widehat{\Delta}_+ &= \{(x, y, z) \in \Delta \mid x = y,\ z \geq 0\},\\
\widehat{\Delta}_- &= \{(x, y, z) \in \Delta \mid x = y,\ z \leq 0\},
\end{aligned}$$

see Figure 5(4). For nonnegative integers i, j and k, we define integral classes $(i, j, k)_\pm$, $(j, k)_0 \in C_\Delta$ to be

$$\begin{aligned}
(i, j, k)_+ &= i(1, 1, 1) + j(0, 1, 0) + k(1, 1, 0) = (i + k, i + j + k, i),\\
(i, j, k)_- &= i(0, 0, -1) + j(0, 1, 0) + k(1, 1, 0) = (k, j + k, -i),\\
(j, k)_0 &= (0, j, k)_+ = (0, j, k)_-,
\end{aligned}$$

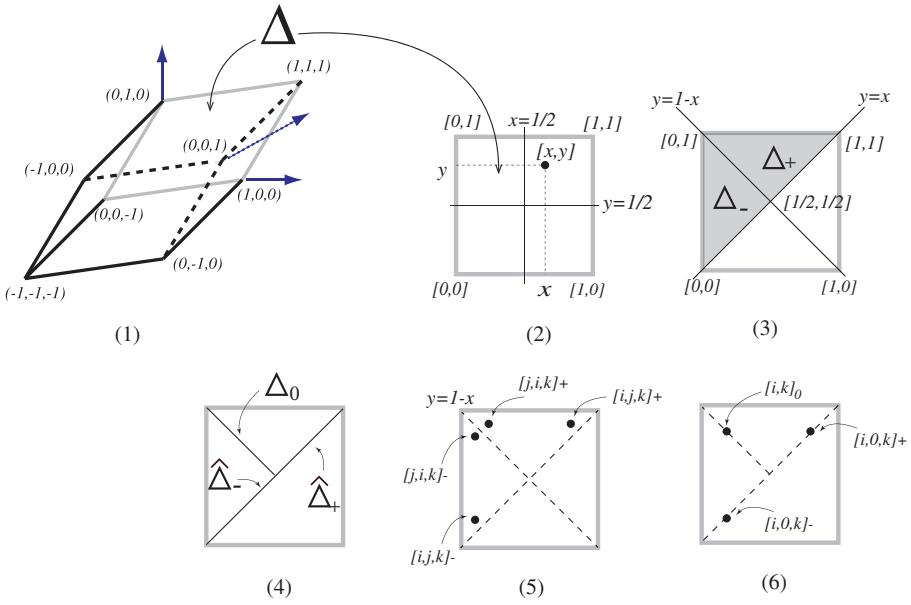

FIGURE 5. (1) Thurston norm ball U_N and the fibered face Δ. (2) $[x, y] \in \Delta$. (3) $\Delta_\pm$. (4) Δ_0, $\widehat{\Delta}_\pm$. (5) Projective classes $[i, j, k]_\pm$ and $[j, i, k]_\pm$. (6) Projective classes $[i, 0, k]_\pm$ and $[i, k]_0 = [0, i, k]_\pm$.

where $(1, 1, 1) = \alpha + \beta + \gamma$, $(0, 0, -1) = -\gamma$, $(0, 1, 0) = \beta$, and $(1, 1, 0) = \alpha + \beta$. The classes $(i, j, k)_\pm$ with $i, j, k > 0$ are said to be *nondegenerate*. Other classes $(i, j, k)_\pm$ are said to be *degenerate*. Note that an integral class $(i, j, k)_\pm$ is fibered if and only if i, j are nonnegative integers and k is a positive integer, see (2.2). If a fibered class $(x, y, z) \in \mathrm{int}(C_\Delta)$ satisfies $y \geq x$ and $z \leq 0$ (resp. $y \geq x$ and $z \geq 0$), then (x, y, z) is written by $(i, j, k)_+$ (resp. $(i, j, k)_-$) for some $i, j \geq 0$ and $k \geq 1$.

We use the notations $f_{(i,j,k)_\pm}$ and $\lambda_{(i,j,k)_\pm}$ in the same manner as $f_{(x,y,z)}$ and $\lambda_{(x,y,z)}$ appeared in Lemma 2.6. We denote by $[a]$, the projection of a to the fibered face Δ. For simplicity, we write $[(i, j, k)_\pm] = [i, j, k]_\pm$ and $[(j, k)_0] = [j, k]_0$. Clearly $[i, j, k]_\pm \in \Delta_\pm$ and $[j, k]_0 \in \Delta_0$. By claims (2)(3) in the following lemma, we find that coordinates $(i, j, k)_\pm$ are useful to study symmetries of the entropy function on N.

Lemma 2.7. *Let $a = (i, j, k)_\pm \in \mathrm{int}(C_\Delta)$ be a primitive integral class.*

(1) *The dilatation $\lambda_{(i,j,k)_\pm}$ is the largest root of*

$$f_{(i,j,k)_\pm}(t) = t^{i+j+2k} - t^k - t^{i+k} - t^{j+k} - t^{i+j+k} + 1.$$

In particular $\lambda_{(i,j,k)_+} = \lambda_{(i,j,k)_-}$.

(2) *The integral class $(j, i, k)_\pm$ is a fibered class in $\mathrm{int}(C_\Delta)$, and the equality $f_{(i,j,k)_\pm} = f_{(j,i,k)_\pm}$ holds. In particular, $\lambda_{(i,j,k)_\pm} = \lambda_{(j,i,k)_\pm}$.*

(3) *Two classes* $[i,j,k]_+$ *and* $[j,i,k]_+$ *have a line symmetry about* $x=\frac{1}{2}$, *and* $[i,j,k]_+$ *and* $[i,j,k]_-$ *have a line symmetry about* $y=-x+1$, *see Figure* 5(5)(6).

Proof. The claim (1) holds by Lemma 2.6(5). The first part of (2) follows from (2.2). The second part of (2) is obvious from the claim (1). The proof of (3) is easy to check. (cf. Corollary 2.7 and Remark 2.8 in [17].) □

Although all fibered classes $(i,j,k)_\pm$ and $(j,i,k)_\pm$ have the same Thurston norm $i+j+2k$ and the same dilatation, the topological types of their fibers could be different. To see what the pseudo-Anosovs $\Phi_{(i,j,k)_\pm}$ and $\Phi_{(j,i,k)_\pm}$ look like, we will see the curve complexes associated to $(i,j,k)_\pm$ and $(j,i,k)_\pm$ in Section 3.7.

3. Construction

In Section 3.1, we construct the pseudo-Anosov homeomorphism on $\Sigma_{0,4}$ which represents the mapping class corresponding to the 3-braid $\sigma_1^2\sigma_2^{-1}$. It serves the monodromy $\Phi_{\alpha+\beta}: F_{\alpha+\beta}\to F_{\alpha+\beta}$ of the fibration on N associated to $\alpha+\beta$, and plays a rule as a pseudo-Anosov homeomorphism Φ in Theorem 2.3. We also construct a train track representative $\mathfrak{p}_{\alpha+\beta}:\tau_{\alpha+\beta}\to\tau_{\alpha+\beta}$ of $\phi_{\alpha+\beta}=[\Phi_{\alpha+\beta}]$.

Oertel used branched surfaces to describe the Thurston norm and to study fibers of fibrations on hyperbolic, fibered 3-manifolds. For basic definitions and results on branched surfaces, see [23, 30, 31]. In Section 3.2, we find minimal representatives of nonfibered classes α, β, $\kappa_\pm$, where $\kappa_+=\alpha+\beta+\gamma$ and $\kappa_-=-\gamma$. In Section 3.3, by using minimal representatives found in Section 3.2, we build two branched surfaces $\mathcal{B}_\pm$ which carry fibers $F_{(i,j,k)_\pm}$ of fibrations associated to any fibered class $(i,j,k)_\pm$. Then in Section 3.4, we construct the train track $\tau_{(i,j,k)_\pm}$ which carries the unstable foliation $\mathcal{F}_{(i,j,k)_\pm}$ of the pseudo-Anosov monodromy $\Phi_{(i,j,k)_\pm}: F_{(i,j,k)_\pm}\to F_{(i,j,k)_\pm}$ of the fibration associated to $(i,j,k)_\pm$. In Section 3.5, we construct the pseudo-Anosov $\Phi_{(i,j,k)_\pm}: F_{(i,j,k)_\pm}\to F_{(i,j,k)_\pm}$ explicitly. In Section 3.6, we give an explicit construction of the train track representative $\mathfrak{p}_{(i,j,k)_\pm}:\tau_{(i,j,k)_\pm}\to\tau_{(i,j,k)_\pm}$ for $\phi_{(i,j,k)_\pm}=[\Phi_{(i,j,i)_\pm}]$. We also construct the directed graph $\Gamma_{(i,j,k)_\pm}$ induced by $\mathfrak{p}_{(i,j,k)_\pm}:\tau_{(i,j,k)_\pm}\to\tau_{(i,j,k)_\pm}$ to indicate where each real edge of $\tau_{(i,j,k)_\pm}$ maps to under $\mathfrak{p}_{(i,j,k)_\pm}$. In Section 3.7, we give the curve complex $G_{(i,j,k)_\pm}$ of $\Gamma_{(i,j,k)_\pm}$ and compute its clique polynomial $Q_{(i,j,k)_\pm}(t)$ whose largest root equals the dilatation $\lambda_{(i,j,k)_\pm}$.

3.1. Fibered class $\boldsymbol{\alpha+\beta}$. Let $L=L_{\mathcal{M}}:\mathbb{R}^2\to\mathbb{R}^2$ be the linear map induced by $\mathcal{M}=\left(\begin{smallmatrix}3&2\\1&1\end{smallmatrix}\right)\in SL(2,\mathbb{Z})$. Since $\mathcal{M}$ has eigenvalues $\lambda^{\pm1}(=2\pm\sqrt{3})$ with $\lambda^+>1$, the linear map L descends to the Anosov diffeomorphism $f=f_{\mathcal{M}}:\mathbb{R}^2/\mathbb{Z}^2\to\mathbb{R}^2/\mathbb{Z}^2$ on the torus. Figure 6 is an illustration of the image of the unit square with the origin (on the left bottom corner) under L.

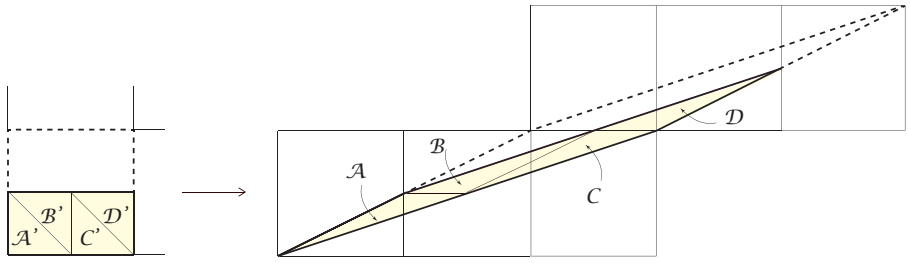

FIGURE 6. Rectangle $\mathcal{R}$ (left) and its image $L(\mathcal{R})$ (right). (The images of the isosceles right-angled triangles $\mathcal{A}'$, $\mathcal{B}'$, $\mathcal{C}'$ and $\mathcal{D}'$ under L are the acute-angled triangles $\mathcal{A}$, $\mathcal{B}$, $\mathcal{C}$ and $\mathcal{D}$.)

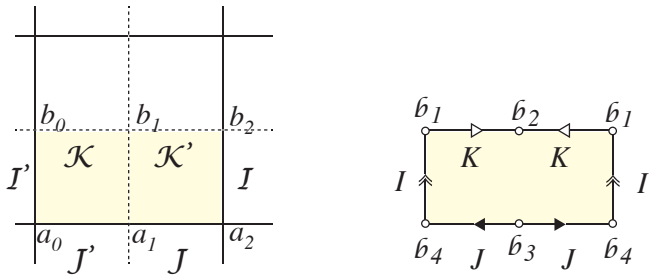

(1) (2)

FIGURE 7. (1) $\mathcal{R} = a_0a_2b_2b_0$. (2) 4-punctured sphere $\mathbb{S} \setminus \mathbb{B}$.

The linear map induced by $\left(\begin{smallmatrix} -1 & 0 \\ 0 & -1 \end{smallmatrix}\right) \in SL(2,\mathbb{Z})$ defines an involution $\mathfrak{r} : \mathbb{R}^2/\mathbb{Z}^2 \to \mathbb{R}^2/\mathbb{Z}^2$. The quotient of $\mathbb{R}^2/\mathbb{Z}^2$ by $\mathfrak{r}$, denoted by $\mathbb{S}$, is homeomorphic to a sphere. ($\mathbb{S}$ is called a *pillowcase* because of its shape.) We set the points $a_i = (\frac{i}{2}, 0)$, $b_i = (\frac{i}{2}, \frac{1}{2}) \in \mathbb{R}^2$. Let $\mathcal{R}$ be the rectangle $a_0a_2b_2b_0$ on $\mathbb{R}^2$, see Figure 7(1). Then $\mathbb{S}$ is obtained from $\mathcal{R}$ by identifying the three pairs of the oriented closed segments $\mathcal{K} = b_0b_1$ with $\mathcal{K}' = b_2b_1$, $\mathcal{I}' = a_0b_0$ with $\mathcal{I} = a_2b_2$, and $\mathcal{J}' = a_1a_0$ with $\mathcal{J} = a_1a_2$, see Figure 7. If we let $\pi : \mathbb{R}^2 \to \mathbb{S}$ be the composition of the projections $\mathbb{R}^2 \to \mathbb{R}^2/\mathbb{Z}^2$ and $\mathbb{R}^2/\mathbb{Z}^2 \to \mathbb{S}$, then the differentiable structure of $\mathbb{S}$ has the four singularities $\mathfrak{b}_1 = \pi(b_0)$, $\mathfrak{b}_2 = \pi(b_1)$, $\mathfrak{b}_3 = \pi(a_1)$ and $\mathfrak{b}_4 = \pi(a_0)$ which lie on the corners of $\mathbb{S}$. We set $\mathbb{B} = \{\mathfrak{b}_1, \mathfrak{b}_2, \mathfrak{b}_3, \mathfrak{b}_4\}$.

We have the identity $f \circ \mathfrak{r} = \mathfrak{r} \circ f$, and this implies that $f : \mathbb{R}^2/\mathbb{Z}^2 \to \mathbb{R}^2/\mathbb{Z}^2$ induces a homeomorphism $\tilde{f} : \mathbb{S} \to \mathbb{S}$. Clearly $\mathbb{B}$ is invariant under $\tilde{f}$. (More concretely, $\tilde{f}(\mathfrak{b}_i) = \mathfrak{b}_i$ for $i = 1, 4$, $\tilde{f}(\mathfrak{b}_2) = \mathfrak{b}_3$ and $\tilde{f}(\mathfrak{b}_3) = \mathfrak{b}_2$.) We see that the homeomorphism $\tilde{f}$ on $\mathbb{S}$ away from $\mathbb{B}$ inherits the (un)stable foliation of the Anosov f. Therefore, $f : \mathbb{R}^2/\mathbb{Z}^2 \to \mathbb{R}^2/\mathbb{Z}^2$ induces a pseudo-Anosov

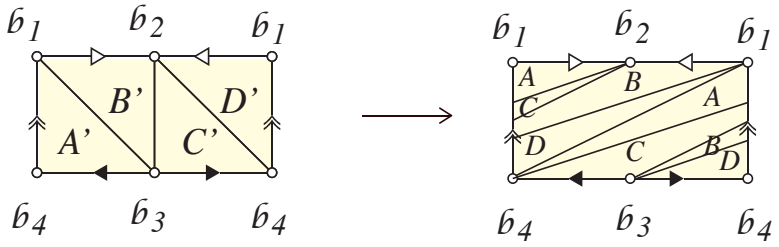

FIGURE 8. $\tilde{f}(=\Phi_{\alpha+\beta}) : \Sigma_{0,4} \to \Sigma_{0,4}$.

homeomorphism on $\mathbb{S} \setminus \mathbb{B} \simeq \Sigma_{0,4}$, see Figure 7(2). Abusing the notation, we denote the pseudo-Anosov on $\mathbb{S} \setminus \mathbb{B}$ by the same notation $\tilde{f}$. Figure 8 is an illustration of $\tilde{f} : \Sigma_{0,4} \to \Sigma_{0,4}$. (cf. Figure 6.) Let A', B', C' and D' be isosceles right-angled triangles whose vertices are punctures of $\Sigma_{0,4}$, see Figure 8(left). Their images under $\tilde{f}$, denoted by A, B, C and D, look as in Figure 8(right).

Observe that the (un)stable foliation of $\tilde{f}$ has a 1-pronged singularity at each puncture. If we regard the puncture $\mathfrak{b}_4$ as the boundary of the 3-punctured disk, then the mapping class $[\tilde{f}]$ is written by a 3-braid on a disk. Since $\mathcal{M}$ is of the form $\left(\begin{smallmatrix}1 & 1\\ 0 & 1\end{smallmatrix}\right)^2 \left(\begin{smallmatrix}1 & 0\\ 1 & 1\end{smallmatrix}\right)$, we see that $[\tilde{f}]$ is represented by the 3-braid $\sigma_1^2\sigma_2^{-1}$ (reading the word from the right to the left). Equivalently $[\tilde{f}]$ is written by $(h_1)^2 \circ h_2^{-1}$, where h_i denotes the mapping class which represents the positive half-twist about the segment $\mathfrak{b}_i\mathfrak{b}_{i+1}$, see Figure 7(2).

Remark 3.1. We have a natural homeomorphism $\tilde{h} : S^3 \setminus \mathrm{br}(\sigma_1^2\sigma_2^{-1}) \to \mathbb{T}_{[\tilde{f}]}$. The cusp of the component K_2' (resp. K_1') of the link $\mathrm{br}(\sigma_1^2\sigma_2^{-1})$ maps to (under $\tilde{h}$) the cusp corresponding to the orbit of $\mathfrak{b}_4$ (resp. $\mathfrak{b}_1$) of the suspension flow (see Figure 1(2)). The cusp of the component K_3' maps to (under $\tilde{h}$) the cusp corresponding to the orbit $\mathfrak{b}_2$ (or $\mathfrak{b}_3$).

By Lemma 2.6(1) together with Remark 3.1, we can regard $\tilde{f} : \Sigma_{0,4} \to \Sigma_{0,4}$ as the monodromy $\Phi_{\alpha+\beta} : F_{\alpha+\beta} \to F_{\alpha+\beta}$ of the fibration on N associated to $\alpha + \beta$. We denote $\tilde{f}$ by $\Phi_{\alpha+\beta}$.

Next we turn to a train track representative of $\phi_{\alpha+\beta} = [\Phi_{\alpha+\beta}]$. Let $\tau_{\alpha+\beta}$ be a train track on $\Sigma_{0,4}$ as in Figure 9(1). Figures 9(1)(5) show that $\tau_{\alpha+\beta}$ is invariant under $\phi_{\alpha+\beta}$. In fact, we have the image $\Phi_{\alpha+\beta}(\tau_{\alpha+\beta})$ in Figure 9(2). (For the illustration of $\Phi_{\alpha+\beta}(\tau_{\alpha+\beta})$, consider the image of the acute-angled triangle B, see Figure 8(right).) The train track $\Phi_{\alpha+\beta}(\tau_{\alpha+\beta})$ is isotopic to the one as in Figure 9(5) which is carried by $\tau_{\alpha+\beta}$. As a result, we get the desired train track representative $\mathfrak{p}_{\alpha+\beta} : \tau_{\alpha+\beta} \to \tau_{\alpha+\beta}$ of $\phi_{\alpha+\beta}$ whose incidence matrix of $\mathfrak{p}_{\alpha+\beta}$ (with respect to the real edges p and q) is equal to $\mathcal{M} = \left(\begin{smallmatrix}3 & 2\\ 1 & 1\end{smallmatrix}\right)$.

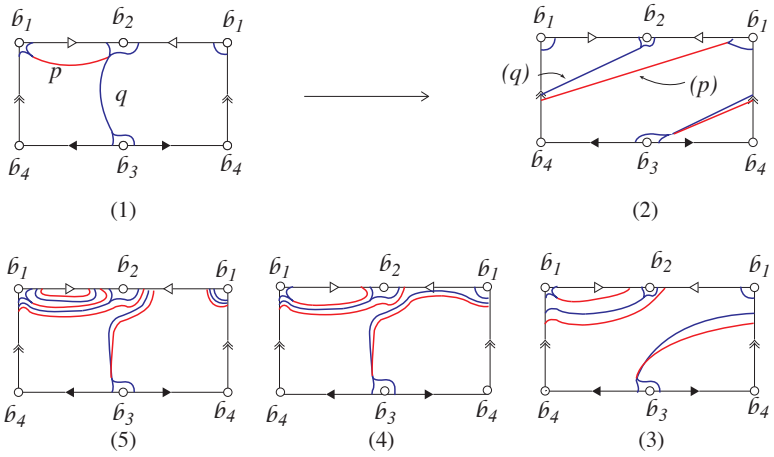

FIGURE 9. (1) Train track $\tau_{\alpha+\beta}$. (2) The image of $\tau_{\alpha+\beta}$ under $\tilde{f}$, where the image of the edge p etc. is denote by (p) etc. The image $\tilde{f}(\tau_{\alpha+\beta})$ can be put in the tie neighborhood of $\tau_{\alpha+\beta}$ under the isotopy, see (2)→(3)→(4)→(5). (From (4) → (5), the edges in (4) that are isotopic to the edges $(p) = \tilde{f}(p)$ and $(q) = \tilde{f}(q)$ in (2) cross over the segment K (see Figure 7(2) for K).

In the rest of the paper, we consider the magic manifold N of the form $\mathbb{T}_{\phi_{\alpha+\beta}} = \Sigma_{0,4} \times [0,1]/\sim$, where $\sim$ identifies $x \times \{1\}$ with $\Phi_{\alpha+\beta}(x) \times \{1\}$ for each $x \in \Sigma_{0,4}$. We investigate the suspension flow $\Phi^t_{\alpha+\beta}$ on $\mathbb{T}_{\phi_{\alpha+\beta}}$. We choose the orientation of $\mathbb{S} \setminus \mathbb{B}$ so that its normal direction coincides with the flow direction of $\Phi^t_{\alpha+\beta}$. We fix the illustration of the 4-punctured sphere $\mathbb{S} \setminus \mathbb{B}$ as in Figure 7(2), and we often omit the names of the punctures $\mathfrak{b}_i$'s in figures.

Remark 3.2. The loop edges of $\tau_{\alpha+\beta}$ surrounding punctures $\mathfrak{b}_1$, $\mathfrak{b}_2$ are $\mathfrak{b}_3$ are infinitesimal edges for $\mathfrak{p}_{\alpha+\beta} : \tau_{\alpha+\beta} \to \tau_{\alpha+\beta}$. Other edges p and q are real edges. Each component of $\Sigma_{0,4} \setminus \tau_{\alpha+\beta}$ is a once punctured monogon. (This comes from the fact that the (un)stable foliation of $\tilde{f}$ has a 1-pronged singularity at each puncture.) In particular the component of $\Sigma_{0,4} \setminus \tau_{\alpha+\beta}$ containing the puncture $\mathfrak{b}_4$ has exactly one cusp.

3.2. Minimal representatives of α, β, $-\gamma$ and $\alpha+\beta+\gamma$. First we define several sets on $\mathbb{R}^2$. Let $\mathcal{T}_A$ and $\mathcal{T}_B$ be the triangles $a_0b_2b_0$ and $a_0a_2b_2$ respectively. Let $\mathcal{P}_{K_-}$ and $\mathcal{P}_{K_+}$ be the parallelograms $a_0a_1b_4b_3$ and $a_1a_2b_5b_4$ respectively. See Figure 10(1). Note that

$$\mathbb{S} = \pi(\mathcal{R}) = \pi(\mathcal{T}_A \cup \mathcal{T}_B) = \pi(\mathcal{P}_{K_-} \cup \mathcal{P}_{K_+}),$$

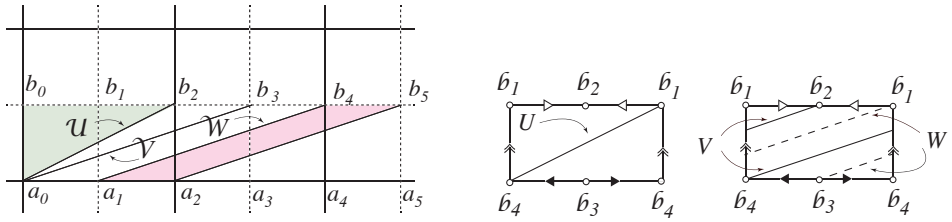

FIGURE 10. (1) $\mathcal{T}_A = a_0b_2b_0$, $\mathcal{T}_B = a_0a_2b_2$, $\mathcal{P}_{K_+} = a_1a_2b_5b_4$, $\mathcal{P}_{K_-} = a_0a_1b_4b_3$, $\mathcal{U} = a_0b_2$, $\mathcal{V} = b_3a_0$, $\mathcal{W} = b_4a_1$. (2) U. (3) V, W.

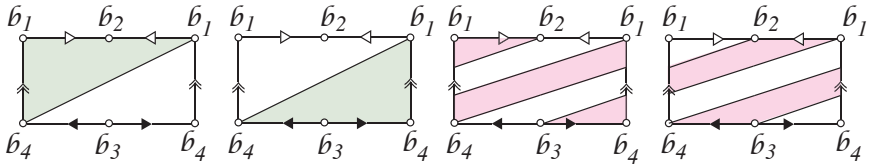

FIGURE 11. (1) T_A. (2) T_B. (3) P_{K_+}. (4) P_{K_-}.

where $\pi : \mathbb{R}^2 \to \mathbb{S}$ is the projection in Section 3.1. Let $\mathcal{U}$ be the oriented closed segment a_0b_2. Let $\mathcal{V}$ and $\mathcal{W}$ be the oriented closed segments b_3a_0 and b_4a_1.

Let T_A be the image $\pi(\mathcal{T}_A) \subset \mathbb{S}$ removing all points in $\mathbb{B}$, i.e., $T_A = \pi(\mathcal{T}_A) \setminus \mathbb{B}$. We define T_B, P_{K_+}, $P_{K_-} \subset \mathbb{S} \setminus \mathbb{B}$ in the same manner. See Figure 11. Similarly, we let

$$I = \pi(\mathcal{I}) \setminus \mathbb{B} = \pi(\mathcal{I}') \setminus \mathbb{B}.$$

Said differently, I is obtained from $\pi(\mathcal{I}) = \pi(\mathcal{I}')$ by removing the end points. We define $J, K, U, V, W \subset \mathbb{S} \setminus \mathbb{B}$ in the same manner. See Figures 7(2) and 10(2)(3). We choose the orientations of T_A, T_B, $P_{K_\pm}$ which coincide with the ones induced by the fiber $F_{\alpha+\beta} = \mathbb{S} \setminus \mathbb{B}$ of the fibration associated to $\alpha + \beta$.

Remark 3.3. We have $U \cap P_{K_+} = U$ and $U \cap P_{K_+} = \emptyset$, see Figures 10(2) and 11(3)(4).

We have $\Phi_{\alpha+\beta}(I) = U$. (We can check the equality by using Figure 6.) This implies that $I^1 = U^0$ in $\mathbb{T}_{\phi_{\alpha+\beta}}$, and hence the flowband $[I^0, U^0]$ with respect to $\Phi^t_{\alpha+\beta}$ is defined. Let

$$F_A = T^0_A \cup [I^0, U^0],$$
$$F_B = T^0_B \cup [I^0, U^0],$$

see Figure 12(1)(2). Observe that the both F_A and F_B are 3-punctured spheres in $\mathbb{T}_{\phi_{\alpha+\beta}}$.

We find two more 3-punctures spheres $F_{K_\pm}$ in $\mathbb{T}_{\phi_{\alpha+\beta}}$. Note that $\pi(\mathcal{J}) = \pi(\mathcal{J}')$ and $\pi(\mathcal{K}) = \pi(\mathcal{K}')$. We have that $\Phi_{\alpha+\beta}(J) = V$ and $\Phi_{\alpha+\beta}(K) = W$, because $\pi(L(\mathcal{J})) = \pi(\mathcal{V})$ and $\pi(L(\mathcal{K})) = \pi(\mathcal{W})$. Hence $J^1 = V^0$ and $K^1 = W^0$ in $\mathbb{T}_{\phi_{\alpha+\beta}}$, and the flowbands $[J^0, V^0]$ and $[K^0, W^0]$ are defined. Let

$$F_{K_+} = P_{K_+} \cup [J^0, V^0] \cup [K^0, W^0],$$
$$F_{K_-} = P_{K_-} \cup [J^0, V^0] \cup [K^0, W^0],$$

see Figure 12(3)(4). We choose orientations of F_A, F_B and $F_{K_\pm}$ so that they are extended by the orientations of T^0_A, T^0_B and $P^0_{K_\pm}$. (Here we identify T^0_A etc. with T_A etc.)

Lemma 3.4. *The 3-punctured spheres F_A, F_B, F_{K_+} and F_{K_-} are minimal representatives of α, β, $\kappa_+(= \alpha + \beta + \gamma)$ and $\kappa_-(= -\gamma)$ respectively.*

Proof of Lemma 3.4. Let m_1, m_2 and m_3 be the meridians of the components K_1, K_2 and K_3 of the 3 chain link $\mathcal{C}_3$. We take oriented simple closed curves S_1, S_2 and S_3 in $\mathbb{T}_{\phi_{\alpha+\beta}} \simeq N$ as in Figure 13. We observe that the images of m_1, m_2 and m_3 under the homeomorphism $H = \tilde{h} \circ h : S^3 \backslash \mathcal{C}_3 \to \mathbb{T}_{\alpha+\beta}$ are S_1, S_2 and S_3 respectively (up to isotopy).

Now, we consider the intersections $i(\cdot, \cdot)$ between the surface F_B and either S_1, S_2 or S_3. We have $i(F_B, S_1) = 0$, $i(F_B, S_2) = 1$, and $i(F_B, S_3) = 0$. These imply that F_B is a minimal representative of β with the Thurston norm 1. By cut and paste construction of the union of surfaces $F_A \cup F_B$ (for this construction of oriented surfaces, see [35, p104]), we obtain a surface which is homeomorphic to $F_{\alpha+\beta} = \mathbb{S} \setminus \mathbb{B}$. Since $\beta = [F_B]$ and $\alpha + \beta = [F_{\alpha+\beta}] = [F_A \cup F_B]$ with the Thurston norm 2, we conclude that F_A is a minimal representative of α with the Thruston norm 1.

Let us consider the intersections between F_{K_-} and either S_1, S_2, or S_3. We have $i(F_{K_-}, S_1) = 0$, $i(F_{K_-}, S_2) = 0$, and $i(F_{K_-}, S_3) = -1$. Thus we conclude that F_{K_-} is a minimal representative of $-\gamma$. Then we see that F_{K_+} is a minimal representative of $\alpha + \beta + \gamma$, because $\alpha + \beta = [F_{\alpha+\beta}]$ and $F_{\alpha+\beta} = \mathbb{S} \setminus \mathbb{B}$ can be obtained from $F_{K_+} \cup F_{K-}$ by cut and paste construction. □

By Lemma 3.4, it makes sense to denote F_A, F_B, F_{K_+} and F_{K_-} by F_α, F_β, F_{κ_+} and F_{κ_-} respectively.

In the end of this subsection, we introduce surfaces F^t_β. We denote by F^t_β, the oriented surface in $\mathbb{T}_{\phi_{\alpha+\beta}}$ which is obtained from F_β by pushing F^0_β along the flow direction for $t \geq 0$ times, see Figure 12(5). Clearly $\beta = [F^t_\beta]$. In the same manner we can define other surfaces $F^t_{\kappa_\pm}$ and $F^t_{\alpha+\beta}$.

3.3. Branched surfaces which carry fibers $F_{(i,j,k)_\pm}$. We first construct the branched surface $\mathcal{B}_+$. Choose $\delta, \epsilon > 0$ with $0 < \delta < 2\delta < 1 - \epsilon$. We

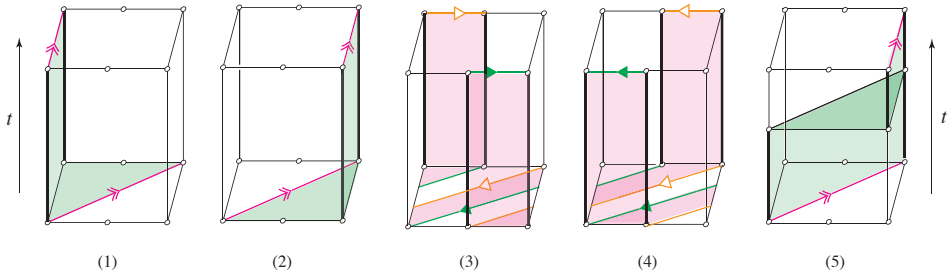

FIGURE 12. (1)–(5) 3-punctured spheres embedded in $\mathbb{T}_{\phi_{\alpha+\beta}}$ with the suspension flow $\Phi^t_{\alpha+\beta}$. The top and bottom surfaces are $\Sigma_{0,4}\times\{1\}$ and $\Sigma_{0,4}\times\{0\}$ respectively. They are identified by $\Phi_{\alpha+\beta}$. Two edges with the same kind (red, green, yellow) are identified in $\mathbb{T}_{\phi_{\alpha+\beta}}$. The vertical arrows with the labeling t indicate the flow directions. (1) $F_\alpha = F_A$. (2) $F_\beta = F_B$. (3) $F_{\kappa_+} = F_{K_+}$. (4) $F_{\kappa_-} = F_{K_-}$. (5) F^t_β for some $0 < t < 1$.

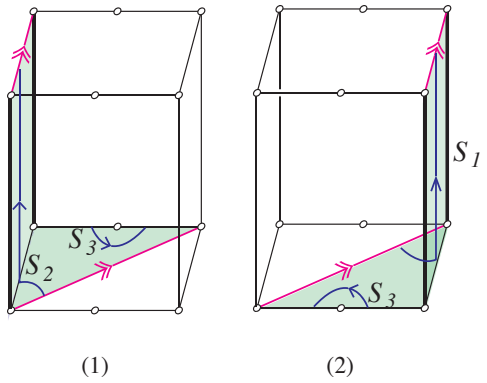

FIGURE 13. (1) S_2, S_3 and F_α in $\mathbb{T}_{\phi_{\alpha+\beta}}$. (2) S_1, S_3 and F_β in $\mathbb{T}_{\phi_{\alpha+\beta}}$.

consider surfaces $F^\delta_{\kappa_+}$, $F^{2\delta}_\beta$, $F^{1-\epsilon}_{\alpha+\beta} \subset \mathbb{T}_{\phi_{\alpha+\beta}}$. We have $\kappa_+ = [F^\delta_{\kappa_+}]$, $\beta = [F^{2\delta}_\beta]$ and $\alpha+\beta = [F^{1-\epsilon}_{\alpha+\beta}]$. Let

$$\widehat{\mathcal{B}}_+ = F^\delta_{\kappa_+} \cup F^{2\delta}_\beta \cup F^{1-\epsilon}_{\alpha+\beta} \subset \mathbb{T}_{\phi_{\alpha+\beta}}. \tag{3.1}$$

The intersection of each pair of the three surfaces is as follows.

(1_+) $F^{1-\epsilon}_{\alpha+\beta} \cap F^{2\delta}_\beta = I^{1-\epsilon}$,

(2_+) $F^{1-\epsilon}_{\alpha+\beta} \cap F^\delta_{\kappa_+} = J^{1-\epsilon} \cup K^{1-\epsilon}$,

(3_+) $F^{2\delta}_\beta \cap F^\delta_{\kappa_+} = J^{2\delta} \cup U^\delta$. (See Remark 3.3 and Figure 12(3)(5).)

The local picture near each intersection looks as in Figure 14(1). A common property of the pairs is that locally, a surface near the intersection is parallel to $F_{\alpha+\beta}$, and it intersects with the flowband which is the subset of the other surface (in fact $F^\delta_{\kappa_+}$ or $F^{2\delta}_\beta$). The branched surface $\mathcal{B}_+$ can be obtained from

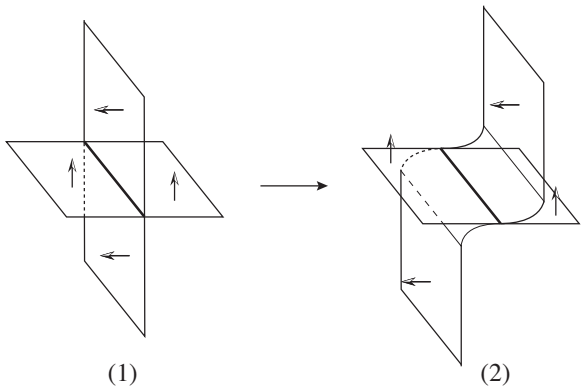

FIGURE 14. (1) Near the intersection of the oriented surfaces (Arrows shows the normal directions). (2) Modification near the intersection which agrees with the orientations of two surfaces.

$\widehat{\mathcal{B}}_+$ by modifying each flowband of $F^{\epsilon}_{\kappa_+}$ and $F^{2\epsilon}_{\beta}$ as in Figure 14(2) so that the modifications agree with the orientations of the two surfaces. Each point in the intersection of surfaces belongs to the *branched locus* of $\mathcal{B}_+$ (that is, the union of points of the branched surface none of whose neighborhood are manifolds).

We build the branched surface $\mathcal{B}_-$ in the same manner: Take $F^{\delta}_{\kappa_-}$ which represents κ_- instead of $F^{\delta}_{\kappa_+}$. Let

$$\widehat{\mathcal{B}}_- = F^{\delta}_{\kappa_-} \cup F^{2\delta}_{\beta} \cup F^{1-\epsilon}_{\alpha+\beta} \subset \mathbb{T}_{\phi_{\alpha+\beta}}. \tag{3.2}$$

We have

(1_-) $F^{1-\epsilon}_{\alpha+\beta} \cap F^{2\delta}_{\beta} = I^{1-\epsilon}$,
(2_-) $F^{1-\epsilon}_{\alpha+\beta} \cap F^{\delta}_{\kappa_-} = J^{1-\epsilon} \cup K^{1-\epsilon}$,
(3_-) $F^{2\delta}_{\beta} \cap F^{\delta}_{\kappa_-} = J^{2\delta}$. (See Remark 3.3 and Figure 12(4)(5).)

The branched surface $\mathcal{B}_-$ is obtained from $\widehat{\mathcal{B}}_-$ by modifying each flowband of $F^{\epsilon}_{\kappa_-}$ and $F^{2\epsilon}_{\beta}$ in the similar manner as in the construction of $\mathcal{B}_+$.

Figure 16(1) (resp. Figure 16(3)) illustrates three pieces (bottom, middle, top) for building $\mathcal{B}_+$ (resp. $\mathcal{B}_-$). In this figure, we have two kinds (solid/broken) of segments without arrows and two kinds (solid/broken) of segments with arrows. The broken segments without arrows are parts of the orbits of punctures $\mathfrak{b}_1$, $\mathfrak{b}_2$, $\mathfrak{b}_3$ and $\mathfrak{b}_4$ (which are circles in the figure) under the flow. In other words, they lie on the cusps of $\mathbb{T}_{\phi_{\alpha+\beta}} \simeq N$. We now explain our convention of Figure 16(1)(3). Firstly, there are some pairs of segments with the same labeling. (Exceptionally, the three segments in Figure 16(1) have the labeling L6.) The two segments with the same labeling mean that one of them is connected to the other with respect to the flow, see Definition 2.4. For the exceptional labeling L6 in Figure 16(1), the

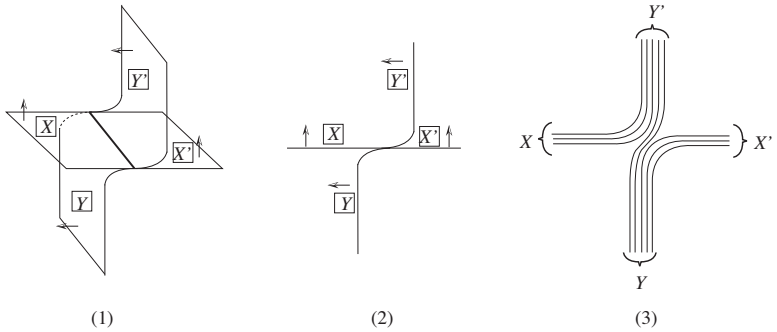

FIGURE 15. (1) Branch equation $X + Y = Y' + X'$. (2) Side view of (1) in this figure. (3) Side view of the surface induced by the branch equation. (In this case $X = X' = 3$, $Y = Y' = 5$.)

bottom segment with the labeling L6 is connected to the middle segment with L6, and the top segment with L6 is connected to the bottom segment with the same labeling. Secondly, we also identify the segment having the labeling $L*$ with the segment having the labeling $L*'$. The result belongs to the branched locus. (For example, the segment with the labeling $L4'$ and the two segments with the labeling $L4$ are identified, and the resulting segment belongs to the branched locus.) Lastly, we can obtain the whole pictures of $\mathcal{B}_\pm$ if we insert a suitable flowband between every two segments with the same labeling. For example, the bottom segment with the labeling $L4$ is connected to the top segment with the same labeling $L4$. We insert a suitable flowband (of the form $[K^{1/3+\epsilon_0}, K^{1-\epsilon}]$) between them. Also the top segment with the labeling 5 is connected to the bottom segment with the same labeling 5. Thus we insert the flowband $[K^1, W^\delta] = [W^0, W^\delta]$ between them. (Note that $K^1 = W^0$ in $\mathbb{T}_{\phi_{\alpha+\beta}}$.) Under the identification of segments and inserting suitable flowbands, each polygon bounded by the solid segments becomes a sector of the branched surface. In general, *sectors* of the branched surface $\mathcal{B}$ are the closures in $\mathcal{B}$ of the components of $\mathcal{B} \setminus$ (the branched locus of $\mathcal{B}$).

We turn to find surfaces carried by $\mathcal{B}_\pm$. To do this, given a fibered class $(i, j, k)_\pm$ (hence $i \geq 0$, $j \geq 0$ and $k \geq 1$), we assign these integers i, j and k for the sectors of $\mathcal{B}_+$ (resp. $\mathcal{B}_-$) as in Figure 16(2) (resp. Figure 16(4)). This is a natural assignment, which we explain the reason now. We assign integers $i \geq 0$, $j \geq 0$ and $k \geq 1$ to $F^\delta_{\kappa_+}$, $F^{2\delta}_\beta$ and $F^{1-\epsilon}_{\alpha+\beta}$ (resp. $F^\delta_{\kappa_-}$, $F^{2\delta}_\beta$ and $F^{1-\epsilon}_{\alpha+\beta}$) consisting of $\widehat{\mathcal{B}}_+$ (resp. $\widehat{\mathcal{B}}_-$). Then we reconstruct $\mathcal{B}_+$ (resp. $\mathcal{B}_-$) with the integers assigned. What we obtain is the assignment of integers in question. Then the branched surface $\mathcal{B}_\pm$ enjoys the branch equations of a particular type such that $X = X'$, $Y = Y'$ and $(X, Y) \in \{(i, j), (j, i), (k, i), (k, j)\}$ as in Figure 15(1). Thus this assignment determines a surface $S_{(i,j,k)_\pm}$ which is

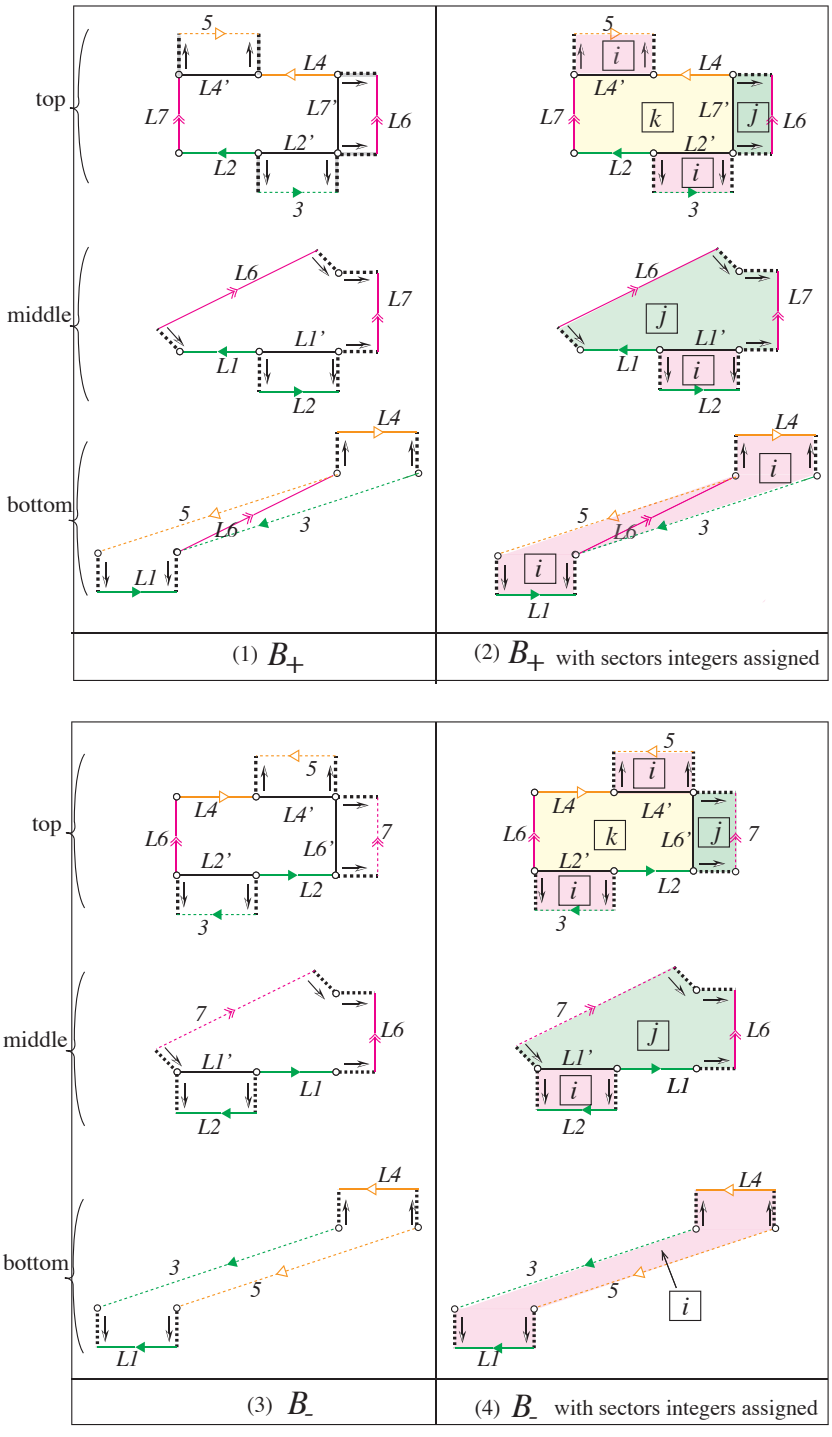

FIGURE 16. (1) Three pieces for building $\mathcal{B}_+$. (2) Assignment of sectors of $\mathcal{B}_+$. (3) Three pieces for building $\mathcal{B}_-$. (4) Assignment of sectors of $\mathcal{B}_-$. The types of arrows (red, green, yellow) are compatible with the ones illustrated in Figure 12.

carried by $\mathcal{B}_\pm$. (See the illustration of Figure 15(3) which shows the surface induced by some branch equation.) Said differently, $S_{(i,j,k)_\pm}$ is obtained from the union

$$\widehat{S}_{(i,j,k)_\pm} = (i \text{ parallel copies of } F_{\kappa_\pm}) \cup (j \text{ parallel copies of } F_\beta) \cup (k \text{ parallel copies of } F_{\alpha+\beta})$$

by cut and paste construction of surfaces (cf. Figure 14). Therefore

$$(i,j,k)_\pm = [S_{(i,j,k)_\pm}].$$

Lemma 3.5. *The surface $S_{(i,j,k)_\pm}$ is the minimal representative of the fibered class $(i,j,k)_\pm$.*

Proof. By definition, $\Delta_\pm$ is a convex hull in Δ containing $\kappa_\pm$ ($\kappa_+ = [1,1]$, $\kappa_- = [0,0]$), $\beta = [0,1]$, $\frac{\alpha+\beta}{2} = [\frac{1}{2},\frac{1}{2}]$, see Figure 5(3). The fibered class $(i,j,k)_\pm$ is in the cone over $\Delta_\pm$, and the surface $S_{(i,j,k)_\pm}$ is built from $\widehat{S}_{(i,j,k)_\pm}$ (which is the union of parallel copies of the minimal representatives $F_{\kappa_\pm}$, F_β and $F_{\alpha+\beta}$) by cut and paste construction. Thus $S_{(i,j,k)_\pm}$ must be the minimal representative of $(i,j,k)_\pm$. □

Remark 3.6. By Lemma 3.5, we write $F_{(i,j,k)_\pm} = S_{(i,j,k)_\pm}$, and $F_{(i,j,k)_\pm}$ becomes a fiber of the fibration associated to $(i,j,k)_\pm$. By Theorem 2.3, $F_{(i,j,k)_\pm}$ (up to isotopy) is transverse to the flow $\Phi^t_{\alpha+\beta}$. The first return map $\Phi_{(i,j,k)_\pm} : F_{(i,j,k)_\pm} \to F_{(i,j,k)_\pm}$ with respect to $\Phi^t_{\alpha+\beta}$ becomes the pseudo-Anosov monodromy of the fibration associated $(i,j,k)_\pm$.

3.4. Train tracks $\tau_{(i,j,k)_\pm}$. We note that the unstable foliation $\mathcal{F}_{\alpha+\beta}$ of $\Phi_{\alpha+\beta}$ is carried by $\tau_{\alpha+\beta}$. Let $\widehat{\mathcal{F}}$ be the suspension of $\mathcal{F}_{\alpha+\beta}$ by $\Phi_{\alpha+\beta}$ which is the 2-dimensional foliation of $\mathbb{T}_{\phi_{\alpha+\beta}}$. We now construct the branched surfaces $\mathcal{B}_{\Delta_\pm}$, each of which carries $\widehat{\mathcal{F}}$. Let δ and ϵ be as in Section 3.3, that is δ and ϵ are constants such that $0 < \delta < 2\delta < 1 - \epsilon$. Hereafter we fix $\delta = \frac{1}{3}$. We choose two families $\{\tau_t^+\}_{0\le t\le 1}$ and $\{\tau_t^-\}_{0\le t\le 1}$ of train tracks with the following properties. (See Figure 17, in which the time t increases along arrows.)

(1) $\tau_0^+ = \tau_0^- = \Phi_{\alpha+\beta}(\tau_{\alpha+\beta})$.
(2) $\tau_t^+ = \tau_t^- = \tau_{\alpha+\beta}$ for $1 - \epsilon_0 \le t \le 1$.
(3) $\tau_t^\pm$ is obtained from $\tau_s^\pm$ by folding edges of $\tau_s^\pm$ for each $0 \le s < t \le 1 - \epsilon$, or $\tau_t^\pm$ is isotopic to $\tau_s^\pm$.
(4) $\tau_t^+ = \tau_t^-$ for $0 \le t \le \frac{2}{3}$, and $\{\tau_t^\pm\}_{0\le t\le\frac{2}{3}}$ is given as in Figure 17(3).
(5) $\{\tau_t^+\}_{\frac{2}{3}<t\le 1-\epsilon}$ (resp. $\{\tau_t^-\}_{\frac{2}{3}<t\le 1-\epsilon}$) is given as in Figure 17(1) (resp. (2)).

In Figure 17, $\sigma \xrightarrow[\text{folding}]{} \tau$ (resp. $\sigma \xrightarrow[\text{isotopy}]{} \tau$) means that τ is obtained from σ by folding edges of σ (resp. τ is isotopic to σ). Observe that nonloop edges of $\tau^+_{1/3} = \tau^-_{1/3}$ (resp. $\tau^+_{2/3} = \tau^-_{2/3}$) do not intersect with V and W (resp. with

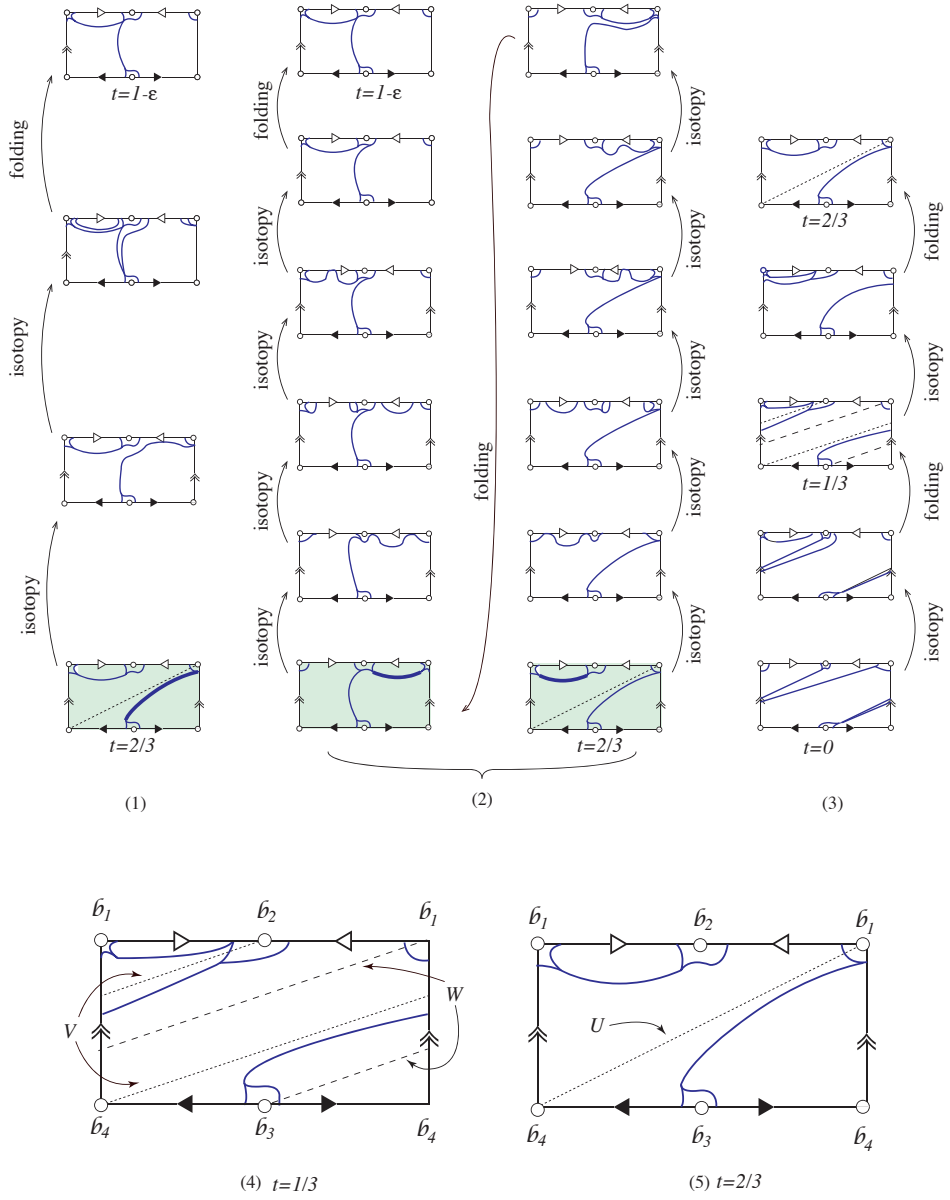

FIGURE 17. (Some of times t are indicated near the puncture $\mathfrak{b}_3$.) (1) $\{\tau_t^+\}_{2/3<t\leq 1-\epsilon}$. (2) $\{\tau_t^-\}_{2/3<t\leq 1-\epsilon}$. (3) $\{\tau_t^\pm\}_{0\leq t\leq 2/3}$. (4) $\tau^+_{1/3}=\tau^-_{1/3}$. (5) $\tau^+_{2/3}=\tau^-_{2/3}$.

U), see Figure 17(4)(5). The branched surfaces $\mathcal{B}_{\Delta_\pm}\subset \mathbb{T}_{\phi_{\alpha+\beta}}$ are defined to be

$$\mathcal{B}_{\Delta_\pm}=\bigcup_{0\leq t\leq 1}\tau_t^\pm\times\{t\}/\sim, \tag{3.3}$$

where $\sim$ identifies $(x,1)$ and $(\Phi_{\alpha+\beta}(x),0)$ for $x \in \tau_{\alpha+\beta}$.

Remark 3.7. The condition (5) and Figure 17 show the difference between $\mathcal{B}_{\Delta_+}$ and $\mathcal{B}_{\Delta_-}$. The conditions (1)–(4) (without (5)) allow us to construct a branched surface which carries $\widehat{\mathcal{F}}$. The reason we require (5) is that it is easy to extract a train track on $F_{(i,j,k)_\pm}$ from the intersection $F_{(i,j,k)_\pm} \cap \mathcal{B}_{\Delta_\pm}$ with the extra condition (5) (see Lemma 3.9(2)).

Remark 3.8. The following analysis is used in the proof of Lemma 3.9(2). It happens twice that an edge of some element in the subfamily $\{\tau_t^-\}_{1/3\le t\le 1-\epsilon}$ is passing through the segment K under the isotopy, see Figure 17(2)(3). On the other hand, the same thing happens once in the subfamily $\{\tau_t^+\}_{1/3\le t\le 1-\epsilon}$, see Figure 17(1)(3). In the same figure, 4-punctured disks containing the track tracks in question are colored, and edges of these train tracks in question are made thick.

Since $F_{(i,j,k)_\pm}$ (up to isotopy) is transverse to the flow $\Phi^t_{\alpha+\beta}$, we may assume that $F_{(i,j,k)_\pm}$ is transverse to $\mathcal{B}_{\Delta_\pm}$. We let

$$\tau'_{(i,j,k)_\pm} = F_{(i,j,k)_\pm} \cap \mathcal{B}_{\Delta_\pm}. \tag{3.4}$$

Lemma 3.9.

(1) *The unstable foliation $\mathcal{F}_{(i,j,k)_\pm}$ of the pseudo-Anosov $\Phi_{(i,j,k)_\pm}$ is carried by $\tau'_{(i,j,k)_\pm}$.*
(2) *Each component of $F_{(i,j,k)_\pm} \setminus \tau'_{(i,j,k)_\pm}$ is either a bigon (a disk with 2 cusps) or a once punctured disk (i.e., annulus) with k cusps for some $k \ge 1$.*

Proof. (1) By Theorem 2.3, we have $\mathcal{F}_{(i,j,k)_\pm} = F_{(i,j,k)_\pm} \cap \widehat{\mathcal{F}}$. Moreover its suspension $\widehat{\mathcal{F}}_{(i,j,k)_\pm}$ by $\Phi_{(i,j,k)_\pm}$ is isotopic to $\widehat{\mathcal{F}}$, see [27, Corollary 3.2]. Since $\widehat{\mathcal{F}}$ is carried by the branched surface $\mathcal{B}_{\Delta_\pm}$, so is $\widehat{\mathcal{F}}_{(i,j,k)_\pm}$. This implies that $\mathcal{F}_{(i,j,k)_\pm}$ is carried by $\tau'_{(i,j,k)_\pm} = F_{(i,j,k)_\pm} \cap \mathcal{B}_{\Delta_\pm}$.

(2) We recall that the suitable branch equations on $\mathcal{B}_\pm$ induce $F_{(i,j,k)_\pm}$. Also recall that we need to insert some flowbands between the two segments with the same labeling to get the whole picture of $\mathcal{B}_\pm$. To view components of $F_{(i,j,k)_\pm} \setminus \tau'_{(i,j,k)_\pm}$, let us consider $\mathcal{B}_\pm \cap \mathcal{B}_{\Delta_\pm}$ on $\mathcal{B}_\pm$ which is a 1-branched manifold. We recall the definition of $\widehat{\mathcal{B}}_\pm$, see (3.1) and (3.2). The constant δ is chosen to be $\frac{1}{3}$, and we have the train tracks $\tau^+_{1-\epsilon} = \tau^-_{1-\epsilon} = \tau_{\alpha+\beta}$, $\tau^+_{2/3} = \tau^-_{2/3}$, $\tau^+_{1/3} = \tau^-_{1/3}$, see Figure 17. Then the 'patterns' in Figure 18(1)(2) are obtained from $\mathcal{B}_\pm \cap \mathcal{B}_{\Delta_\pm}$ after folding or splitting all edges which appear on the flowbands. In fact the thick edge e_+ in Figure 18(1) is the one (resp. thick edges e'_- and e''_- in Figure 18(2) are the ones) by folding some edge (resp. by splitting some edges) which appear(s) on the flowband between the segments with the labeling $L4$, see also Remark 3.8. Then we reconstruct the fibers $F_{(i,j,k)_\pm}$ obtained from the suitable branch equations on $\mathcal{B}_\pm$ with

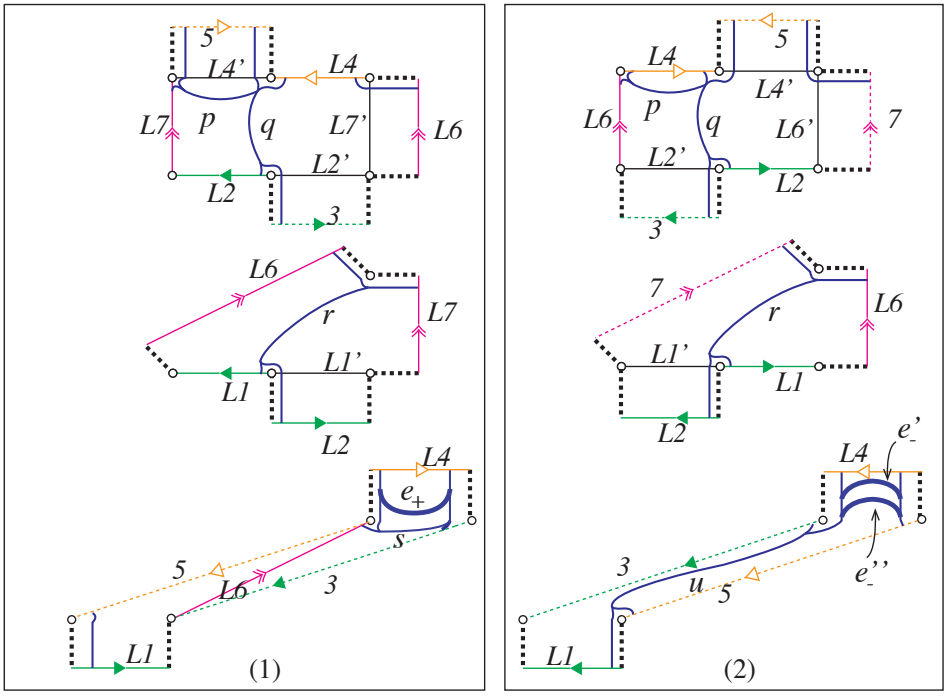

FIGURE 18. (1) $\mathcal{B}_+ \cap \mathcal{B}_{\Delta_+}$. (2) $\mathcal{B}_- \cap \mathcal{B}_{\Delta_-}$. (cf. Figure 16(1)(3).)

the 'patterns' in Figure 18(1)(2) . That we get is $\tau'_{(i,j,k)_\pm}$ (up to folding and splitting the edges) on $F_{(i,j,k)_\pm}$. Each edge of $\tau'_{(i,j,k)_\pm}$ originates in some edge of the branched 1-manifold $\mathcal{B}_\pm \cap \mathcal{B}_{\Delta_\pm}$. We denote some of the edges of $\mathcal{B}_+ \cap \mathcal{B}_{\Delta_+}$ (resp. $\mathcal{B}_- \cap \mathcal{B}_{\Delta_-}$) by p, q, r, s (resp. p, q, r, u) as in Figure 18(1) (resp. (2)).

We can fold all edges of $\tau'_{(i,j,k)_+}$ (resp. $\tau'_{(i,j,k)_-}$) which originate in e_+ (resp. e'_- or e''_-) into some edges. This means that these edges lie on the boundaries of some components of $F_{(i,j,k)_\pm} \setminus \tau'_{(i,j,k)_\pm}$ that are bigons. We fold all these edges as much as possible (i.e., collapse bigons), and we consider complementary regions of the resulting 1-branched manifold. The combinatorics from Figures 16(2)(4) and 18 tell us that each component of the resulting 1-branched manifold is a once punctured disk with k cusps for some $k \geq 1$. □

Let $\tau_{(i,j,k)_\pm}$ be the branched 1-manifold obtained from $\tau'_{(i,j,k)_\pm}$ by collapsing all bigons of $\tau'_{(i,j,k)_\pm}$. By Lemma 3.9, we immediately have:

Lemma 3.10. *$\tau_{(i,j,k)_\pm}$ is a train track on $F_{(i,j,k)_\pm}$ which carries $\mathcal{F}_{(i,j,k)_\pm}$.*

3.5. Monodromies $\Phi_{(i,j,k)_\pm} : F_{(i,j,k)_\pm} \to F_{(i,j,k)_\pm}$ of the fibrations associated to $(i,j,k)_\pm$. First of all, we represent fibers $F_{(i,j,k)_\pm}$ more

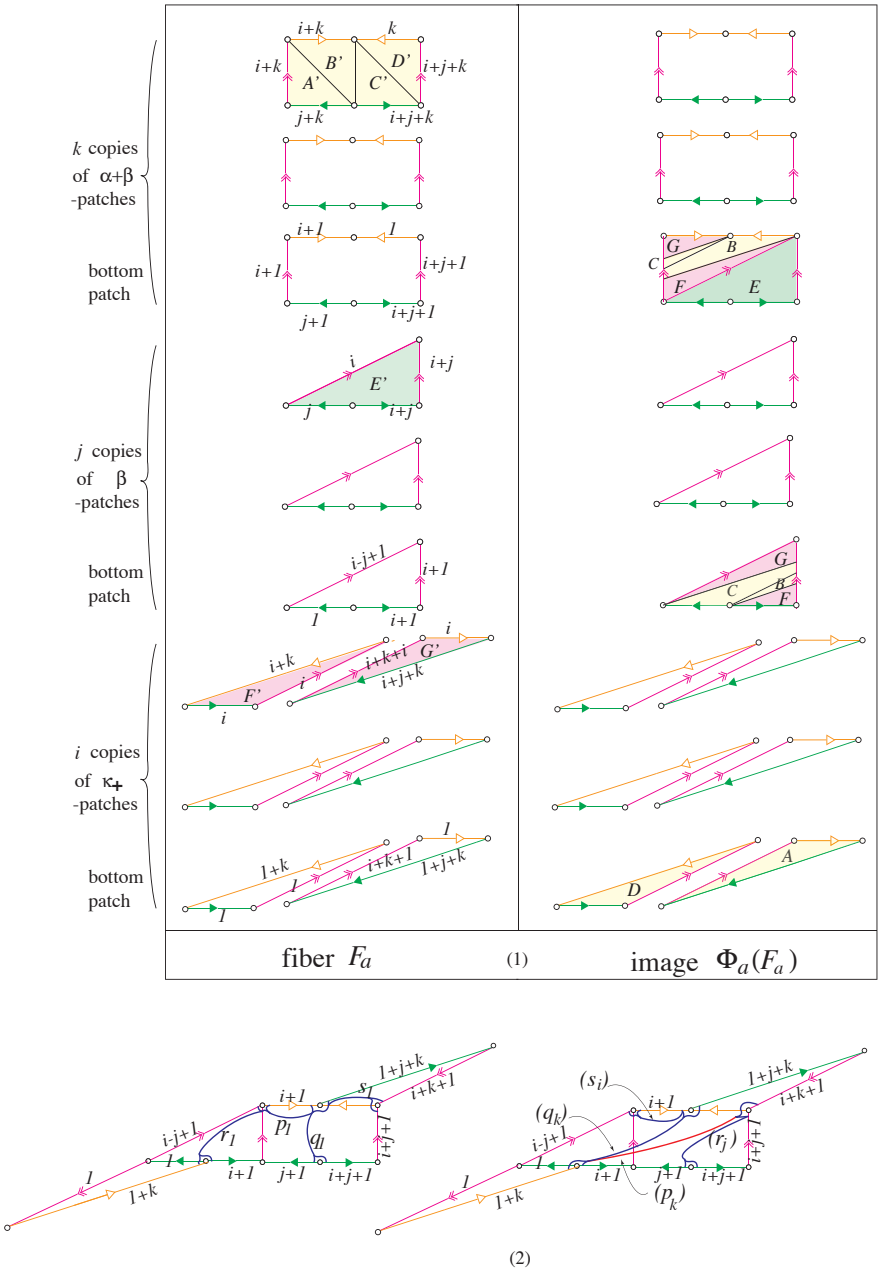

FIGURE 19. Labeling of segments in the right column of (1) is the same as the one in the left column. (1) $\Phi_a : F_a \to F_a$ for nondegenerate $a = (i, j, k)_+$. (2) (left) Bottom edges s_1, r_1, p_1 and q_1 which lie on three bottom patches. (right) Images of top edges s_i, r_j, p_k and q_k under Φ_a which lie on three bottom patches. We denote by (s_i) etc., the image $\Phi_a(s_i)$ etc.

simpler as follows. We shrink each flowband of $F_{(i,j,k)_\pm}$ as much as possible along flow lines into some edge. (Note that this operation does not change the topological types of fibers.) Said differently, we simplify the branched surfaces $\mathcal{B}_\pm$ as follows. Shrink each flowband of the three pieces, see Figure 16(1) (resp. (3)), as much as possible along flow lines into some edge. Then the branch equations on $\mathcal{B}_\pm$ induce the one on such a simplified branched surface, from which one gets a surface in question which is homeomorphic to $F_{(i,j,k)_\pm}$.

After shrinking flowbands, the resulting three pieces (the bottom, middle, top pieces) are:

(1) κ_+-patch: the two acute-angled triangles sharing vertices $\mathfrak{b}_1$ and $\mathfrak{b}_4$ (resp. κ_--patch: the parallelogram),
(2) β-patch: the right-angled triangle, and
(3) $\alpha+\beta$-patch: the rectangle.

We call these pieces (1) *κ_+-patch* (resp. *κ_--patch*), (2) *β-patch* and (3) *$\alpha+\beta$-patch*. See Figure 19(1) (resp. Figure 20(1)) for three kinds of patches. We often draw pairs of the two acute-angled triangles for the κ_+-patch separately as in Figure 19(1), but they should share the two vertices $\mathfrak{b}_1$ and $\mathfrak{b}_4$ (cf. Figure 11(3)). We can get the simplified fibers $F_{(i,j,k)_+}$ (resp. $F_{(i,j,k)_-}$) from i parallel copies of κ_+-patches (resp. κ_--patches), j parallel copies of β-patches and k parallel copies of $\alpha+\beta$-patches under suitable identifications of the boundaries of patches.

If we have j parallel copies of the same kind of patch, say β-patches, $\mathbb{P}^1_\beta, \cdots, \mathbb{P}^j_\beta$, we have $\mathbb{P}^\ell_\beta \subset F^{n_\ell}_{\alpha+\beta}$ for some $0 < n_\ell < 1$, where $\ell \in \{1, \cdots, j\}$. For the notation of $F^{n_\ell}_{\alpha+\beta}$, see the end of Section 3.2. If $0 < n_1 < \cdots < n_{j-1} < n_j < 1$, then we call the β-patch $\mathbb{P}^1_\beta$ *the bottom (β-)patch*, and call $\mathbb{P}^j_\beta$ *the top (β-)patch*. Other β-patches are called *the middle (β-)patches*. We define the top, middle, bottom for other patches similarly. We color each top of the three kinds of patches, see Figure 19(1)(left column), Figure 20(1)(left column). Here we label E' for the top β-patch, and label F' and G' (resp. F') for the top κ_+-patch (resp. κ_--patch) in the same figure. We label A', B', C' and D' for isosceles right-angled triangles which lie on the top $\alpha+\beta$-patch.

The patches needed for building $F_{(i,j,k)_\pm}$ for the nondegenerate class $(i,j,k)_\pm$ are given as in the same figure. We can think three kinds of patches are in the cylinder $\Sigma_{0,4} \times (0,1) \subset \mathbb{T}_{\phi_{\alpha+\beta}}$. We have the flow direction in the cylinder from the 'bottom' $\Sigma_{0,4} \times \{0\}$ to the 'top' $\Sigma_{0,4} \times \{1\}$. The types of arrows (red, green, yellow) in the figure are compatible with the ones illustrated in Figures 12 and 16. Among the patches with the same kind ($\kappa_\pm$-patches, β-patches or $\alpha+\beta$-patches), the way to label parallel segments with the same kind of arrow is that the number for the labeling increases (cyclically) along the flow direction. We often omit to label segments which lie on the middle patches. To get the fiber $F_{(i,j,k)_\pm}$, we identify the two

segments with the same kind of arrow and with the same labeling (same number) by using the flow $\Phi^t_{\alpha+\beta}$. In the right column of (1) in the same figure, the labeling of segments on patches are the same as the one given in the left column.

Let us turn to construct $\Phi_{(i,j,k)_\pm} : F_{(i,j,k)_\pm} \to F_{(i,j,k)_\pm}$ explicitly. It is enough to describe where each patch maps to. Since the desired monodromy $\Phi_{(i,j,k)_\pm}$ is the first return map on $F_{(i,j,k)_\pm}$ with respect to $\Phi^t_{\alpha+\beta}$, we see the following. All patches but the top of each kind of patch map to the next above patch (of the same kind) along the flow direction. Thus the monodromy $\Phi_{(i,j,k)_\pm}$ restricted to these patches is just a shift map. On the other hand, each top patches map to some bottom patches (possibly with different kinds), see Figure 19(1) for $\Phi_{(i,j,k)_+}$ and see Figure 20(1) for $\Phi_{(i,j,k)_-}$, where $A, B, \cdots$ are the images of $A', B', \cdots$ under $\Phi_{(i,j,k)_\pm}$. More precisely, we can get the image of the top β-patch under $\Phi_{(i,j,k)_\pm}$ when we push the fiber $F_{(i,j,k)_\pm}$ along the flow direction and see how this top patch hits to the bottom $\alpha+\beta$-patch. Similarly, one can get the image of the top κ_+-patch (resp. top κ_--patch) under $\Phi_{(i,j,k)_+}$ (resp. $\Phi_{(i,j,k)_-}$) if we see how this top patch hits to the both bottom β-patch and bottom $\alpha+\beta$-patch. To get the images of the isosceles right-angled triangles A', B', C' and D' which lie on the top $\alpha+\beta$-patch, we first consider the acute-angled triangles A, B, C and D which lie on $\Sigma_{0,4}\times\{0\}$ as in Figure 8(right). Then investigate how these acute-angled triangles hit bottoms patches, when we push them along the flow direction.

The monodromies of the fibrations associated to the degenerate classes can be constructed similarly. As an example, we deal with the degenerate classes $a=(j,k)_0$'s, see Figure 21.

Remark 3.11. Suppose that $(j,k)_0$ is primitive (i.e., $\gcd(j,k)=1$). Then the fiber $F_{(j,k)_0}$ is connected, and it has genus 0, see [18]. Many pseudo-Anosovs with small dilatations defined on the surfaces of genus 0 are contained in the family of fibered classes $(j,k)_0$'s, see Examples 4.6, 4.7 and [18, Section 4.1]. By using the Artin generators of the braid groups, the words which represent $\phi_{(j,k)_0}$'s are given in [18, Theorem 3.4]. They are quite simple words.

3.6. Train track representatives $\mathfrak{p}_{(i,j,k)_\pm} : \tau_{(i,j,k)_\pm} \to \tau_{(i,j,k)_\pm}$ of $\phi_{(i,j,k)_\pm}$. In the following lemma, we refer to the metrized, directed graph $\Gamma_{(i,j,k)_\pm}$ given in Figures 22 and 23, where each edge with no labeling means that its length is equal to 1, and all edges with labeling are made thick in the figures.

Lemma 3.12.

(1) *The train track $\tau_{(i,j,k)_\pm}$ is invariant under $\phi_{(i,j,k)_\pm} = [\Phi_{(i,j,k)_\pm}]$. If we let $\mathfrak{p}_{(i,j,k)_\pm} : \tau_{(i,j,k)_\pm} \to \tau_{(i,j,k)_\pm}$ be the train track representative of $\phi_{(i,j,k)_\pm}$, then its incidence matrix is Perron–Frobenius.*

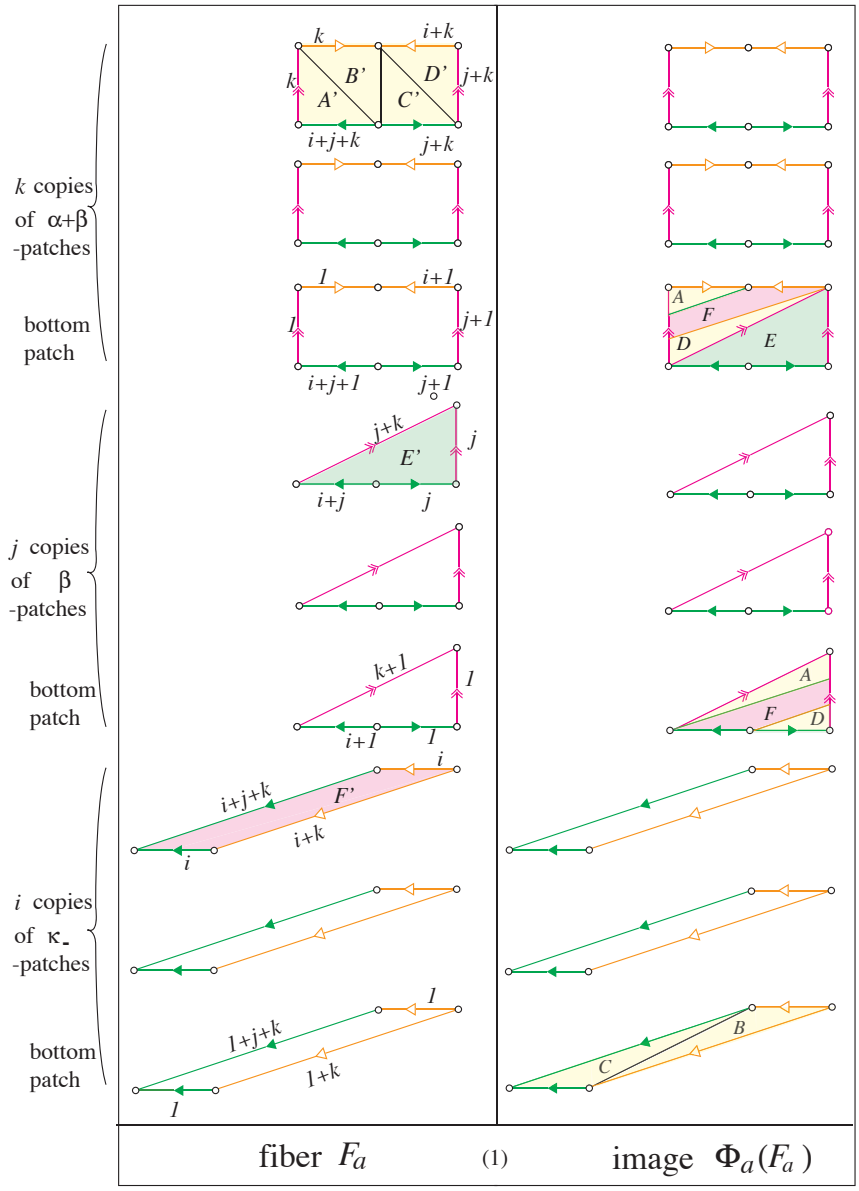

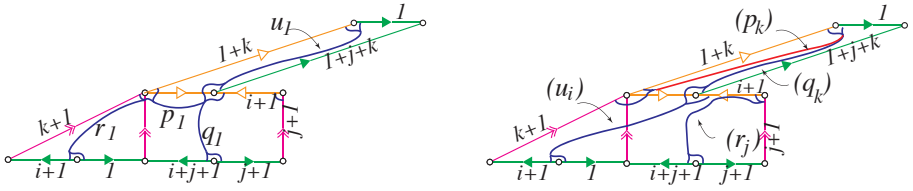

(2)

FIGURE 20. $\Phi_a : F_a \to F_a$ for degenerate $a = (j,k)_0$.

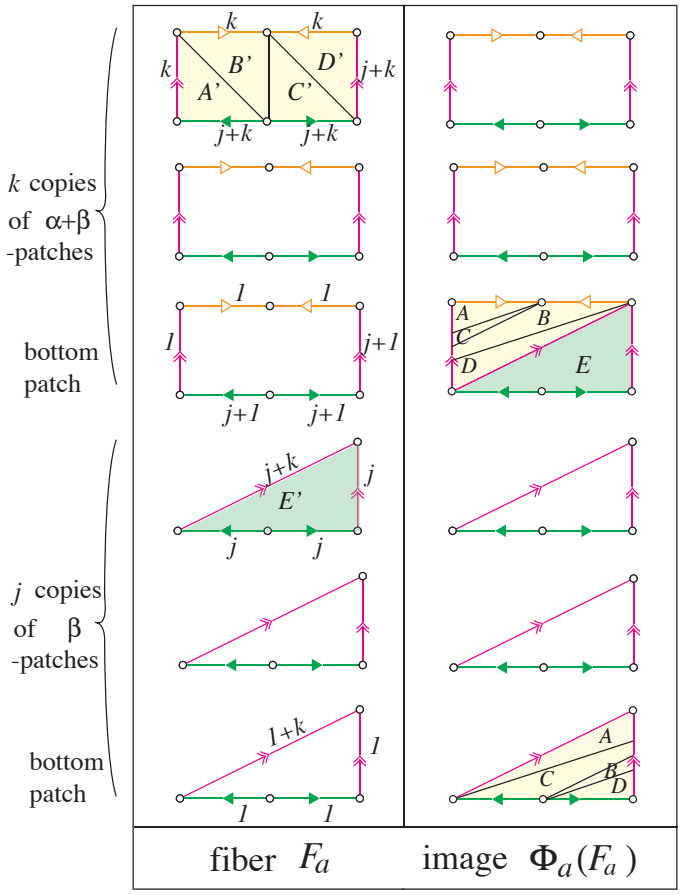

FIGURE 21. $\Phi_a : F_a \to F_a$ for degenerate $a = (j,k)_0$.

(2) *The directed graph* $\Gamma_{(i,j,k)_\pm}$ *is the one induced by*

$$\mathfrak{p}_{(i,j,k)_\pm} : \tau_{(i,j,k)_\pm} \to \tau_{(i,j,k)_\pm}.$$

Once we prove that $\tau_{(i,j,k)_\pm}$ is invariant under $\phi_{(i,j,k)_\pm}$, the claim that the incidence matrix of $\phi_{(i,j,k)_\pm}$ is Perron–Frobenius follows from Theorem 2.1.

Proof of Lemma 3.12. By construction of $\tau_{(i,j,k)_\pm}$, each edge of $\tau_{(i,j,k)_\pm}$ originates in some edge of the intersection $\mathcal{B}_\pm \cap \mathcal{B}_{\Delta_\pm}$ (see Figure 18). We only label edges of $\tau_{(i,j,k)_+}$ (resp. $\tau_{(i,j,k)_-}$) which originate in the edges p, q, r and s (resp. p, q, r and u), since it turns out that the images of other edges under $\Phi_{(i,j,k)_\pm}$ are eventually periodic up to isotopy. We first explain the way to label the edges of $\tau_{(i,j,k)_\pm}$, which is similar to the one to label segments of patches given in Section 3.5. We label parallel edges of $\tau_{(i,j,k)_\pm}$ (which originate in the same edge of $\mathcal{B}_\pm \cap \mathcal{B}_{\Delta_\pm}$) so that the number for the labeling increases along the flow direction. For example, see Figures 30–36.

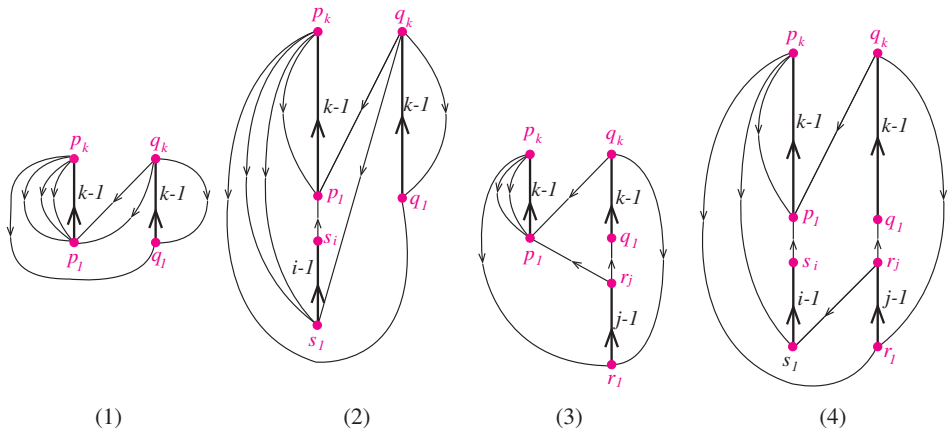

FIGURE 22. Γ_a for $a = (i, j, k)_+$. (1)(2)(3) degenerate cases. (4) nondegenerate case. (1) $a = (0, k)_0$ with $k > 0$. (2) $a = (i, 0, k)_+$ with $i, k > 0$. (3) $a = (j, k)_0$ with $j, k > 0$. (4) $a = (i, j, k)_+$ with $i, j, k > 0$.

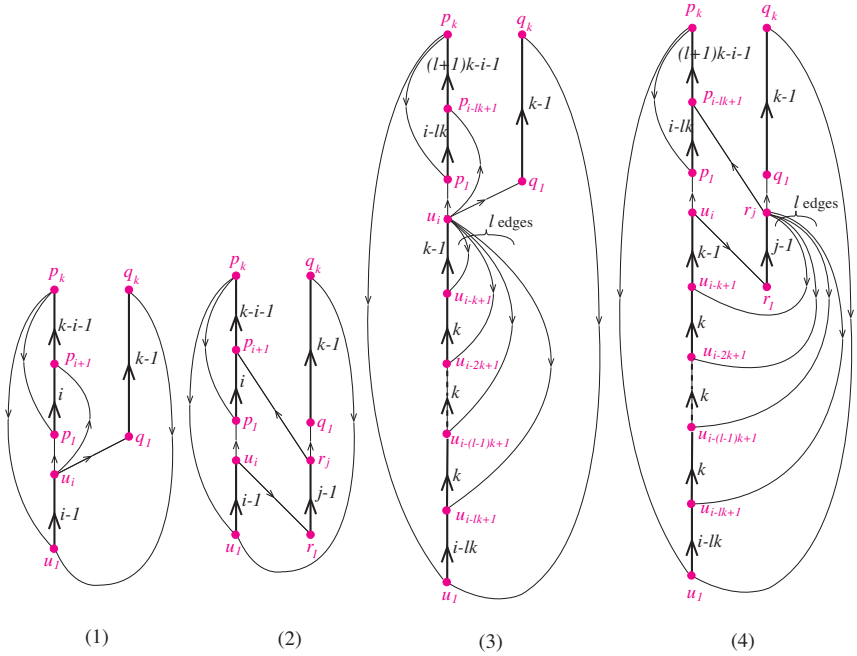

FIGURE 23. Γ_a for $a = (i, j, k)_-$. (1)(3) degenerate cases. (2)(4) nongenerate cases. (1) $a = (i, 0, k)_-$ with $0 < i < k$. (2) $a = (i, j, k)_-$ with $0 < i < k$. (3) $a = (i, 0, k)_-$ with $i \geq k > 0$. (4) $a = (i, j, k)_-$ with $i \geq k > 0$. For (3)(4), $\ell \geq 1$ is an integer such that $0 \leq i - k\ell \leq k - 1$.

We only prove the claims (1) and (2) for nondegenerate classes $(i,j,k)_\pm$. (Proofs for degenerate classes are similar.) Let us describe the image of an edges e with labeling under $\Phi_{(i,j,k)_\pm}$. Such an edge e lies on some patch for building $F_{(i,j,k)_\pm}$. Suppose that e lies on a patch, say $\mathbb{P}_e$ which is not a top patch. Then e maps (under $\Phi_{(i,j,k)_\pm}$) to the next above edge e' which lies on the same kind of patch $\mathbb{P}_{e'}$ as $\mathbb{P}_e$. Clearly, e and e' originate in the same edge of $\mathcal{B}_\pm \cap \mathcal{B}_{\Delta_\pm}$. Suppose that an edge $e_{\rm top}$ of $\tau_{(i,j,k)_\pm}$ lies on some top patch. We call $e_{\rm top}$ the *top edge*. If an edge $e_{\rm bot}$ of $\tau_{(i,j,k)_\pm}$ lies on some bottom patch, then we call $e_{\rm bot}$ the *bottom edge*.

We first consider the nondegenerate class $(i,j,k)_+$. Let us consider the images $\Phi_{(i,j,k)_+}(e_{\rm top})$'s for all top edges $e_{\rm top}$'s. Then we can put $\Phi_{(i,j,k)_+}(e_{\rm top})$'s in the tie neighborhood of $\tau_{(i,j,k)_+}$ which are transverse to the ties up to isotopy, where the support of the isotopy can be taken on the neighborhood of the three bottom patches, see Figure 19(2). Thus $\tau_{(i,j,k)_+}$ is invariant under $\phi_{(i,j,k)_+}$. In fact we can get the edge path $\mathfrak{p}_{(i,j,k)_+}(e_{\rm top})$ from Figure 19(2): The left of (2) of the same figure illustrates the union of all bottom edges of $\tau_{(i,j,k)_+}$ which lies on the union of all bottom patches. The right of (2) of the same figure shows the image of all top edges under $\Phi_{(i,j,k)_+}$. One can find from the right in (2) of the same figure that $\mathfrak{p}_{(i,j,k)_+}(p_k)$ and $\mathfrak{p}_{(i,j,k)_+}(q_k)$ pass through the three edges r_1, p_1, s_1, and the two edges r_1, p_1 respectively. The edge path $\mathfrak{p}_{(i,j,k)_+}(r_j)$ passes through the two edges q_1, s_1.

Note that by Remark 3.2, we see that edges of $\tau_{(i,j,k)_+}$ which originate in the edges p,q,r and s are real edges for $\mathfrak{p}_{(i,j,k)_+}$. Others are infinitesimal edges. We explain a structure of the directed graph in Figure 22(4). If e is one of edges (with some label) which are made thick in the figure, then the end points of e are the vertices having the same origin (p, q, r or s) on $\mathcal{B}_+$. Suppose that e is an edge whose length equals $k-1$, and suppose that e has end points p_1 and p_k having the same origin p. Then the edge e with labeling $k-1$ corresponds to the following edge path with length $k-1$:

$$p_1 \to p_2 \to \cdots \to p_{k-1} \to p_k.$$

In particular all vertices between p_1 and p_k have the same origin p on $\mathcal{B}_+$. Putting these things together, we can check that metrized, directed graph $\Gamma_{(i,j,k)_+}$ in Figure 22(4) is the one induced by $\mathfrak{p}_{(i,j,k)_+} : \tau_{(i,j,k)_+} \to \tau_{(i,j,k)_+}$.

We turn to the nondegenerate class $(i,j,k)_-$. In the same manner as in the class $(i,j,k)_+$, we can see that $\tau_{(i,j,k)_-}$ is invariant under $\phi_{(i,j,k)_-}$. The edges of $\tau_{(i,j,k)_-}$ which originate in the edges p,q,r and u are real edges for the train track representative $\mathfrak{p}_{(i,j,k)_-}$ of $\phi_{(i,j,k)_-}$. Others are infinitesimal edges. A hint to obtain $\mathfrak{p}_{(i,j,k)_-}(e_{\rm top})$ is given in Figure 20(2). The left of (2) in the same figure illustrates the union of all bottom edges of $\tau_{(i,j,k)_-}$ which lies on the union of all bottom patches. The right of (2) in the same figure shows the image of all top edges under $\Phi_{(i,j,k)_-}$. The images under $\mathfrak{p}_{(i,j,k)_-}$ of all top edges but r_j are edge paths written by bottom edges. For example, $\mathfrak{p}_{(i,j,k)_-}(u_i)$ is an edge path which passes through r_1 and p_1.

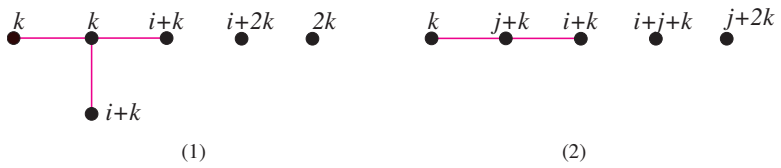

FIGURE 24. G_a for $a = (i,j,k)_+$. (1) $G_a = K^{**}_{1,3}$ if $a = (i,0,k)_+$ including the case $i = 0$ and $k > 0$, see Figure 22(1)(2). (2) $G_a = K^{**}_{1,2}$ if $a = (i,j,k)_+$ including the case $i = 0$, $j > 0$ and $k > 0$, see Figure 22(3)(4).

On the other hand, to put $\Phi_{(i,j,k)_-}(r_j)$ in the tie neighborhood of $\tau_{(i,j,k)_-}$ one needs to make $\Phi_{(i,j,k)_-}(r_j)$ (up to isotopy) across the segment K. An analysis to identify boundaries of patches for building $F_{(i,j,k)_-}$ enables us to get the image $\mathfrak{p}_{(i,j,k)_-}(r_j)$. We can verify that the directed graph $\Gamma_{(i,j,k)_-}$ given in Figure 23(2) (resp. (4)) is the one induced by $\mathfrak{p}_{(i,j,k)_-}$ if $0 < i < k$ (resp. $i \geq k > 0$). The edge path $\mathfrak{p}_{(i,j,k)_-}(r_j)$ has length $\ell + 2$, where $\ell \geq 0$ is an integer such that $0 \leq i - k\ell \leq k - 1$. □

Remark 3.13. Metrized and directed graphs $\Gamma_{(i,j,k)_\pm}$ for nondegenerate classes can recover ones for degenerate classes. See Figures 18(1)(2)(3) and 22(1)(3). To see this, consider $\Gamma_{(i,j,k)_+}$ for the nondegenerate class $(i,j,k)_+$. We have the edge $p_k \to s_1$ and the edge path from s_1 to p_1 for $\Gamma_{(i,j,k)_+}$, see Figure 22(4). Connecting these edge paths, we have the edge path from p_k to p_1 with length > 1, see Figure 22(4). This determines *the edge* $p_k \to p_1$ with length 1 in the degenerate class $(0,j,k)_+ = (j,k)_0$ by 'eliminating' vertices $s_1, \cdots, s_i$, see Figure 22(3). Another example is the following. We have the edge $r_j \to s_1$ and the edge path from s_1 to p_1 for the nondegenerate class $(i,j,k)_+$, see Figure 22(4). They determine *the edge* $r_j \to p_1$ with length 1 for the degenerate class $(0,j,k)_+ = (j,k)_0$, see Figure 22(3).

3.7. Curve complexes $G_{(i,j,k)_\pm}$ and clique polynomials $Q_{(i,j,k)_\pm}(t)$.

We define some graphs. Let $K_{m,n}$ denote the complete bipartite graph with m and n vertices. We denote by $K^{**}_{m,n}$, the disjoint union of $K_{m,n}$ and the graph with two vertices and with no edges.

The metrized, directed graphs $\Gamma_{(i,j,k)_+}$'s and $\Gamma_{(i,j,k)_-}$'s were given in Section 3.6. Here we exhibit their curve complexes $G_{(i,j,k)_+}$'s in Figure 24 and $G_{(i,j,k)_-}$'s in Figure 25. In the next proposition, we give the clique polynomial $Q_{(i,j,k)_\pm}$. We find that it is exactly equal to the polynomial $f_{(i,j,k)_\pm}(t)$ in Lemma 2.7(1).

Proposition 3.14. *The clique polynomial $Q_{(i,j,k)_\pm}(t)$ of the curve complex $G_{(i,j,k)_\pm}$ is the following reciprocal polynomial*

$$Q_{(i,j,k)_\pm}(t) = 1 - (t^k + t^{i+k} + t^{j+k} + t^{i+j+k}) + t^{i+j+2k}.$$

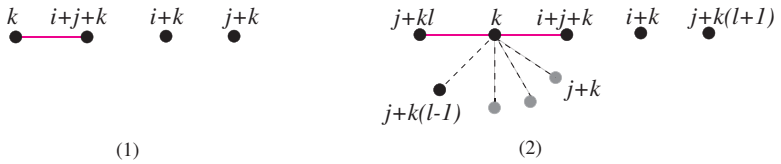

FIGURE 25. G_a for $a = (i,j,k)_-$. (1) $G_a = K^{**}_{1,1}$ if $a = (i,j,k)_-$ with $0 < i < k$ including the case $j = 0$, see Figure 23(1)(2). (2) $G_a = K^{**}_{1,\ell+1}$ if $a = (i,j,k)_-$ with $i \geq k > 0$ including the case $j = 0$, see Figure 23(3)(4). Here $\ell \geq 1$ is an integer such that $0 \leq i - k\ell \leq k-1$. The weights of $\ell+1$ vertices of the subgraph $K_{1,\ell+1}$ surrounding the centered vertex are given by $i+j+k$, $j+k, \cdots, j+k(\ell-1), j+k\ell$ clockwise.

In particular $\lambda_{(i,j,k)_+} = \lambda_{(i,j,k)_-}$ *is the largest root of*

$$Q_{(i,j,k)_+}(t) = Q_{(i,j,k)_-}(t).$$

Proof. It is straightforward to compute the clique polynomial $Q_{(i,j,k)_\pm}(t)$. The dilatation $\lambda_{(i,j,k)_\pm}$ equals the growth rate of $\Gamma_{(i,j,k)_\pm}$. By Theorem 2.5, $\frac{1}{\lambda_{(i,j,k)_\pm}}$ is the smallest root of $Q_{(i,j,k)_\pm}(t)$. Note that $Q_{(i,j,k)_\pm}(t)$ is a reciprocal polynomial, i.e., $Q_{(i,j,k)_\pm}(t) = t^{i+j+2k} Q_{(i,j,k)_\pm}(t^{-1})$. Thus the largest root of $Q_{(i,j,k)_\pm}(t)$ equals $\lambda_{(i,j,k)_\pm}$. □

Proof of Theorem 1.2. Let a be a fibered class of N. By a symmetry of the Thurston norm ball U_N and by Lemma 2.6(4), we may suppose that a is of the form $(i,j,k)_\pm \in \mathrm{int}(C_\Delta)$. Suppose that $a = (0,0,1)_\pm = (0,1)_0$. In this case, we have constructed $\Phi_a : F_a \to F_a$ and $\mathfrak{p}_a : \tau_a \to \tau_a$ explicitly in Section 3.1.

Let us consider other fibered classes $a = (i,j,k)_\pm$'s. The explicit construction of the monodromy $\Phi_a : F_a \to F_a$ of the fibration associated to a is given in Section 3.5. If a is primitive, then the explicit construction of the desired train track representative $\mathfrak{p}_a : \tau_a \to \tau_a$ of ϕ_a together with the induced directed graph Γ_a of $\mathfrak{p}_a$ (Figures 22 and 23) is given in Section 3.6. □

4. A catalogue of small dilatation pseudo-Anosovs

4.1. Fibered classes of Dehn fillings $N(r)$. Recall that T_β (resp. T_α, T_γ) is a torus which is the boundary of a regular neighborhood of the component K_2 (resp. K_1, K_3) of the 3 chain link $\mathcal{C}_3$. Recall that $N(r)$ is the manifold obtained from N by Dehn filling the cusp along the slope $r \in \mathbb{Q} \cup \{\infty\}$. It is known by Martelli-Petronio [25] that $N(r)$ is hyperbolic unless $r \in \{\infty, -3, -2, -1, 0\}$. The manifolds $N(\frac{3}{-2})$ and $N(\frac{1}{-2})$ are the exterior of the Whitehead sister link (i.e., $(-2,3,8)$-pretzel link) and the exterior of the 3-braided link $\mathrm{br}(\sigma_1^{-1}\sigma_2)$ (or 6_2^2 link in the Rolfsen's table)

respectively. Also $N(1)$ is the exterior of the Whitehead link (see [25] for example). These Dehn fillings $N(\frac{3}{-2})$, $N(\frac{1}{-2})$ and $N(1)$ play an important rule to study pseudo-Anosovs with small dilatations (see [17]), which we recall quickly in Section 4.3.

First of all, we consider the relation of fibered classes between N and Dehn fillings $N(r)$'s. We suppose that $N(r)$ is the manifold obtained from N by Dehn filling the cusp specified by T_β along the slope r. By using Lemma 2.6(2) (which says that the boundary slope of $\partial_\beta F_a$ equals $\frac{z+x}{-y}$), we have the following: There exists a natural injection

$$\iota_\beta : H_2(N(r), \partial N(r)) \to H_2(N, \partial N)$$

whose image equals $S_\beta(r)$, where

$$S_\beta(r) = \{(x, y, z) \in H_2(N, \partial N) \mid -ry = z + x\},$$

see [17, Proposition 2.11]. We choose $r \in \mathbb{Q}$ with $r \notin \{-3, -2, -1, 0\}$, and let $a \in S_\beta(r) = \operatorname{Im} \iota_\beta$ be a fibered class in $H_2(N, \partial N)$. Then

$$\overline{a} = \iota_\beta^{-1}(a) \in H_2(N(r), \partial N(r))$$

is also a fibered class of $N(r)$. This is because the monodromy $\Phi_a : F_a \to F_a$ of the fibration on N associated to a extends to the monodromy $\overline{\Phi}_a$ of the fibration on $N(r)$ associated to $\overline{a}$ by capping each boundary component of $\partial_\beta F_a$ with the disk. If the (un)stable foliation $\mathcal{F}_a$ of Φ_a has a property such that each component of $\partial_\beta F_a$ has no 1 prong, then $\mathcal{F}_a$ extends canonically to the (un)stable foliation $\overline{\mathcal{F}}_a$ of $\overline{\Phi}_a$, and hence $\overline{\Phi}_a$ becomes a pseudo-Anosov homeomorphism with the same dilatation as Φ_a. We sometimes denote $N(r)$ by $N_\beta(r)$ when we need to specify the cusp which is filled. By using this notation, we may write $\overline{a} \in H_2(N_\beta(r), \partial N_\beta(r))$.

Similarly, when $N(r)$ is the manifold obtained from N by Dehn filling the cusp specified by another torus T_γ along the slope r, we have a natural injection,

$$\iota_\gamma : H_2(N(r), \partial N(r)) \to H_2(N, \partial N)$$

whose image is given by

$$S_\gamma(r) = \{(x, y, z) \in H_2(N, \partial N) \mid -rz = x + y\}.$$

4.2. Concrete examples. In the following example, we consider some fibered classes a and compute their dilatations $\lambda(a)$. We also exhibit $\tau_a \subset F_a$, its image $\Phi_a(\tau_a)$ putting into the tie neighborhood $\mathcal{N}(\tau_a)$ (so that it is transverse to the ties) and the directed graph $(\Gamma_a, \mathbf{1})$.

Example 4.1.

(1) If $a = (1, 4, 1)_+ = (2, 6, 1)$, then $\lambda(a) \approx 1.7220$ is the largest root of

$$Q_{(1,4,1)_+}(t) = f_{(2,6,1)}(t) = (t^3 + 1)(t^4 - t^3 - t^2 - t + 1).$$

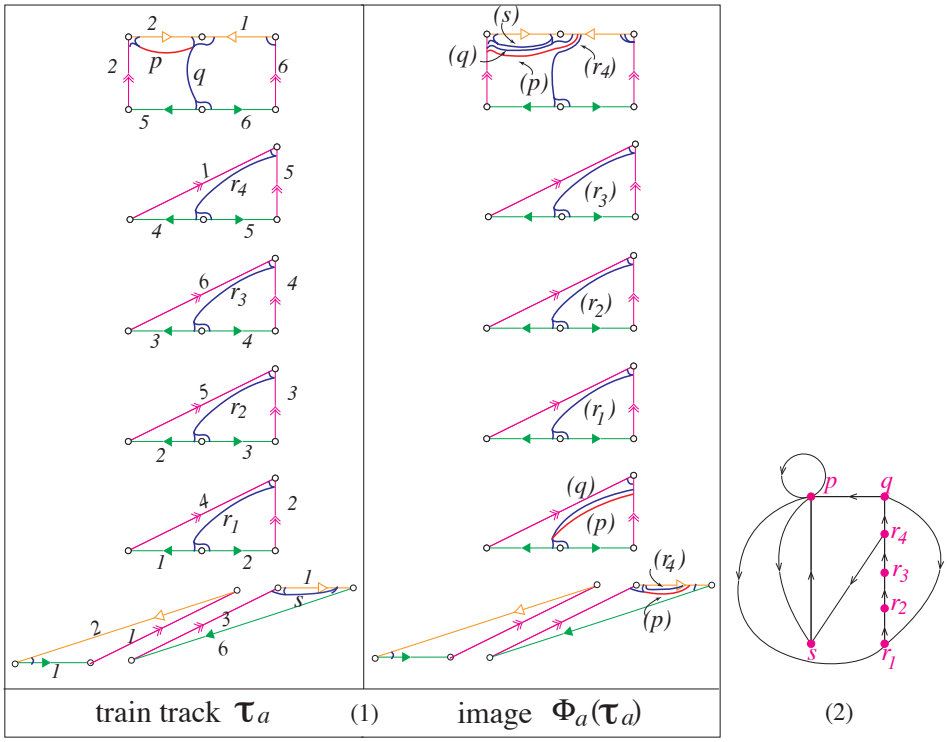

FIGURE 26. (1) $\tau_a \subset F_a$ and $\Phi_a(\tau_a)$ (up to isotopy) (2) Γ_a for $a = (1,4,1)_+$.

By Lemma 2.6(3), F_a has topological type $\Sigma_{2,5}$. By Lemma 2.6(7), $\mathcal{F}_a$ is orientable. This implies that the monodromy $\Phi_a : F_a \to F_a$ of the fibration associated to a extends to the pseudo-Anosov

$$\widehat{\Phi}_a : \widehat{F}_a \to \widehat{F}_a$$

on the closed surface of genus 2 with orientable invariant foliations by capping each boundary component of F_a with the disk. The dilatation of $\widehat{\Phi}_a$ is the same as that of Φ_a, that is $\lambda(a)$. The minimal dilatations δ_2 and δ_2^+ are computed in [4] and [39] respectively, and $\delta_2 = \delta_2^+$ holds. In fact, δ_2 is the largest root of $t^4 - t^3 - t^2 - t + 1$, and hence we have $\lambda(a) = \delta_2 = \delta_2^+$. Thus $\widehat{\Phi}_a$ is a minimizer of $\delta_2 = \delta_2^+$. See Figure 26.

(2) If $a = (3,1,1)_- = (1,2,-3)$, then $\lambda(a) \approx 1.7816$ is the largest root of

$$Q_{(3,1,1)_-}(t) = f_{(1,2,-3)}(t) = t^6 - t^5 - t^4 - t^2 - t + 1.$$

See Figure 27.

(3) If $a = (2,3)_0 = (3,5,0)$, then $\lambda(a) \approx 1.4134$ is the largest root of

$$Q_{(2,3)_0}(t) = f_{(3,5,0)}(t) = t^8 - 2t^5 - 2t^3 + 1.$$

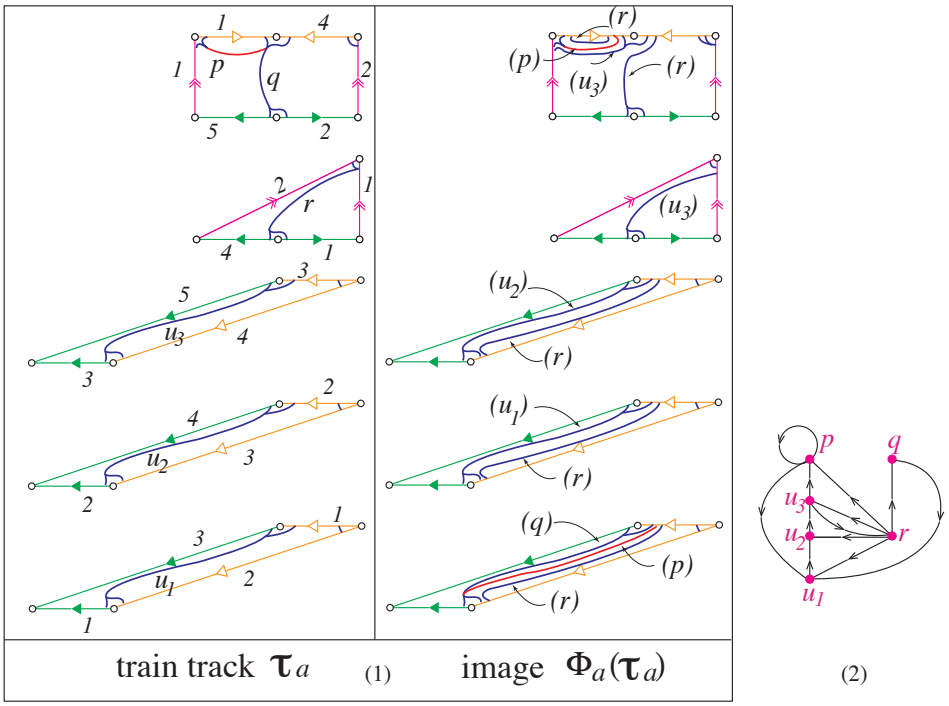

FIGURE 27. (1) $\tau_a \subset F_a$ and $\Phi_a(\tau_a)$ (up to isotopy) (2) Γ_a for $a = (3,1,1)_-$.

The fiber F_a is homeomorphic to $\Sigma_{0,10}$. On the other hand,

$$\sharp(\partial_\alpha F_a) = \sharp(\partial_\beta F_a) = 1,$$

and $\mathcal{F}_a$ has a property such that each component of $\partial_\alpha F_a \cup \partial_\beta F_a$ has no 1 prong. Hence by capping either $\partial_\alpha F_a$ or $\partial_\beta F_a$ with the disk, we get the pseudo-Anosov $\overline{\Phi}_a : \overline{F}_a \to \overline{F}_a$ on the $(8+1)$-punctured sphere with the same dilatation as $\lambda(a)$. Since $\overline{\Phi}_a$ fixes the boundary component ($\partial_\alpha F_a$ or $\partial_\beta F_a$) of F_a, it defines the pseudo-Anosov on D_8. Lanneau and Thiffeault computed $\delta(D_8)$ in [22]. We see that $\lambda(a)$ is equal to $\delta(D_8)$, and hence $\overline{\Phi}_a$ is a minimizer of $\delta(D_8)$. See Figure 28.

4.3. Infinite sequences of fibered classes. We exhibit several infinite sequences of fibered classes of N, each of which corresponds to a subsequence of pseudo-Anosovs to give the upper bounds (U1)–(U6) except (U3) in Table 1. Each sequence lies on the section either $S_\beta(r)$ for $r \in \{\frac{3}{-2}, -1, \frac{1}{-2}\}$ or $S_\gamma(r)$ for $r \in \{1, \infty\}$. A sequence of fibered classes in $S_\beta(\frac{3}{-2})$ (resp. $S_\gamma(1)$, $S_\beta(\frac{1}{-2})$) defines the sequence of fibered classes of the hyperbolic Dehn filling $N(\frac{3}{-2})$ (resp. $N(1)$, $N(\frac{1}{-2})$). We indicate where each sequence sits on the fibered face Δ, see Figure 29. The purpose of the following examples is to

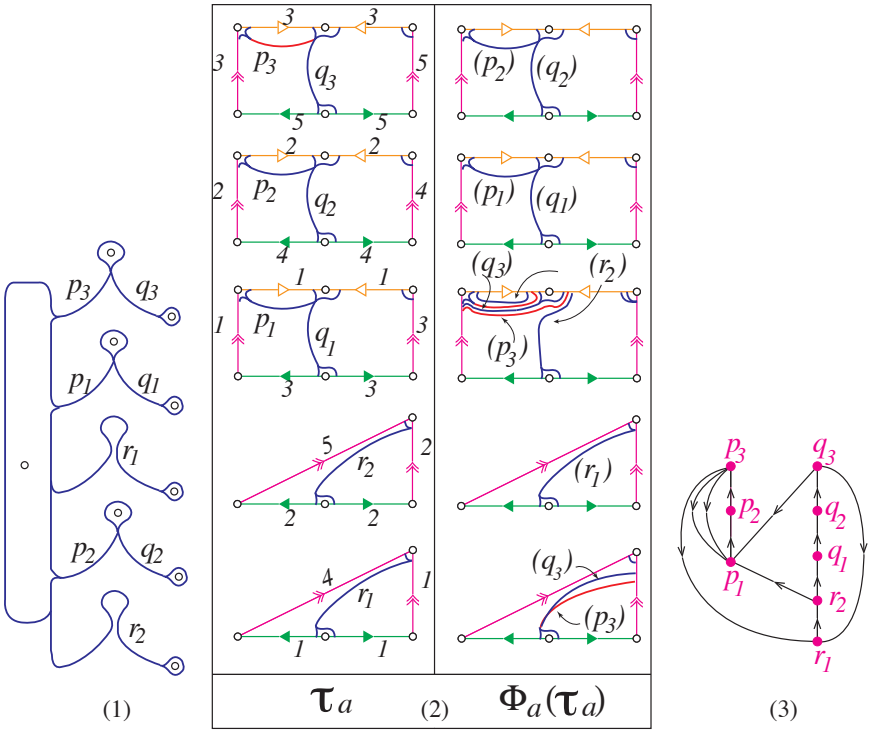

FIGURE 28. (1) τ_a (2) Another description of $\tau_a \subset F_a$ and $\Phi_a(\tau_a)$ (up to isotopy) (3) Γ_a for $a = (2,3)_0$.

construct the invariant train track τ_a, the induced directed graph Γ_a and curve complex G_a associated to each fibered class a in each infinite sequence concretely and to see a structure of the monodromy Φ_a of the fibration associated to a via the curve complex G_a. We will see that the topological type of G_a is fixed, and it is either $K^{**}_{1,2}$ or $K^{**}_{1,3}$ for each infinite sequence. Other sequences of fibered classes of N with small dilatations can be found in [16, Section 5].

Example 4.2 (Figure 30)**.** Suppose that $g \equiv 2, 4 \pmod 6$. Take a sequence of primitive fibered classes

$$a_g = (1, g+2, g-1)_+ = (g, 2g+2, 1) \in S_\beta(\tfrac{1}{-2}).$$

(The fibered class in Example 4.1(1) is a_2 in the present example.) Observe that the projections $[a_g]$'s go to $[\frac{1}{3}, \frac{2}{3}] \in \mathrm{int}(\Delta)$ as g goes to ∞, see Figure 29(1). By Lemma 2.6(3)(7), it was shown in [20] that the fiber F_{a_g} has genus g, and $\mathcal{F}_{a_g}$ is orientable. The dilatation $\lambda_{(1,g+2,g-1)_+}$ is equal to the largest root of

$$Q_{(1,g+2,g-1)_+}(t) = (t^{g+1}+1)(t^{2g} - t^{g+1} - t^g - t^{g-1} + 1).$$

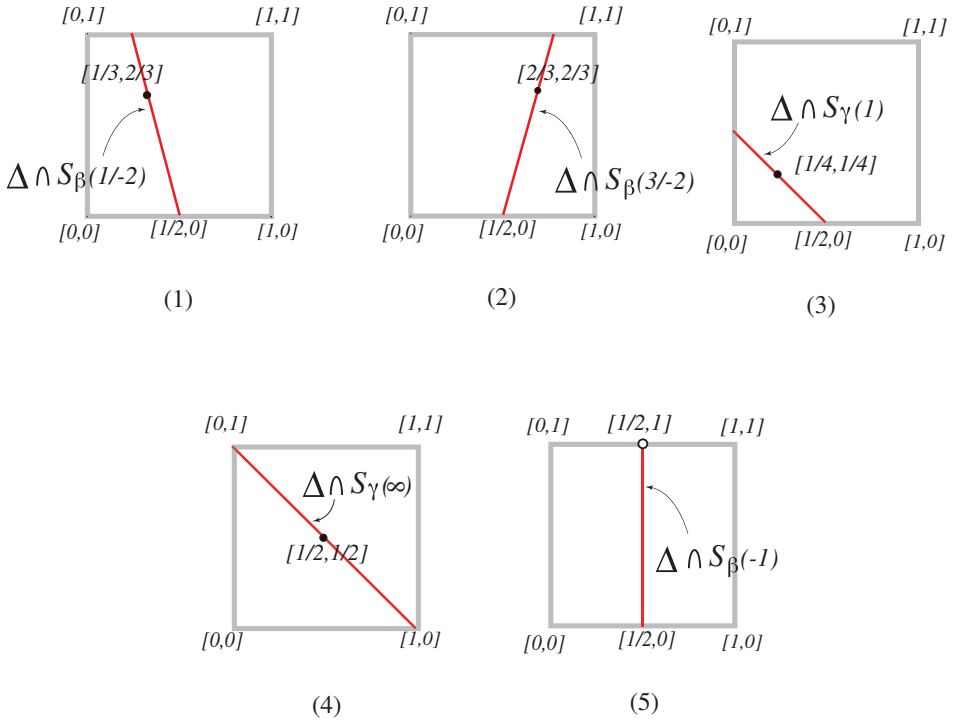

FIGURE 29. (1) $\Delta \cap S_\beta(\frac{1}{-2})$. (2) $\Delta \cap S_\beta(\frac{3}{-2})$. (3) $\Delta \cap S_\gamma(1)$. (4) $\Delta \cap S_\gamma(\infty) = \Delta_0$. (5) $\Delta \cap S_\beta(-1)$.

Since $\mathcal{F}_{a_g}$ is orientable, the monodromy $\Phi_{a_g} : F_{a_g} \to F_{a_g}$ of the fibration associated to a_g extends canonically to the pseudo-Anosov homeomorphism $\widehat{\Phi}_g$ on the closed surface Σ_g of genus g with the dilatation $\lambda_{(1,g+2,g-1)_+}$. We now introduce the *Lanneau–Thiffeault polynomial*

$$f_{(a,b)}(t) = t^{2a} - t^{a+b} - t^a - t^{a-b} + 1.$$

Then $f_{(g,1)}(t)$ is a factor of $Q_{(1,g+2,g-1)_+}(t)$. If we set $\lambda_{(g,1)}$ to be the largest root of $f_{(g,1)}(t)$, then we have $\lambda_{(g,1)} = \lambda_{(1,g+2,g-1)_+} = \lambda(\widehat{\Phi}_g)$. It is known that $\delta_2^+ = \lambda_{(2,1)}$ [39], $\delta_4^+ = \lambda_{(4,1)}$ [21] and $\delta_8^+ = \lambda_{(8,1)}$ [21, 10]. Lanneau and Thiffeault asked in [21] whether the equality $\delta_g^+ = \lambda_{(g,1)}$ holds for even g. The existence of pseudo-Anosovs $\widehat{\Phi}_g$ for $g \equiv 2, 4 \pmod 6$ in the present example were discovered by Hironaka in [10], see also Remark 1.3. The sequence of pseudo-Anosovs $\{\widehat{\Phi}_g\}$ can be used as a subsequence to prove both upper bounds (U1) and (U2) in Table 1. In fact we have

$$\lim_{g\to\infty} g \log \lambda(\widehat{\Phi}_g) = \log(\tfrac{3+\sqrt{5}}{2}).$$

Example 4.3 (Figure 31)**.** An explicit value of δ_7^+ is known. The lower bound of δ_7^+ was given in [21] and an example which realizes this lower bound

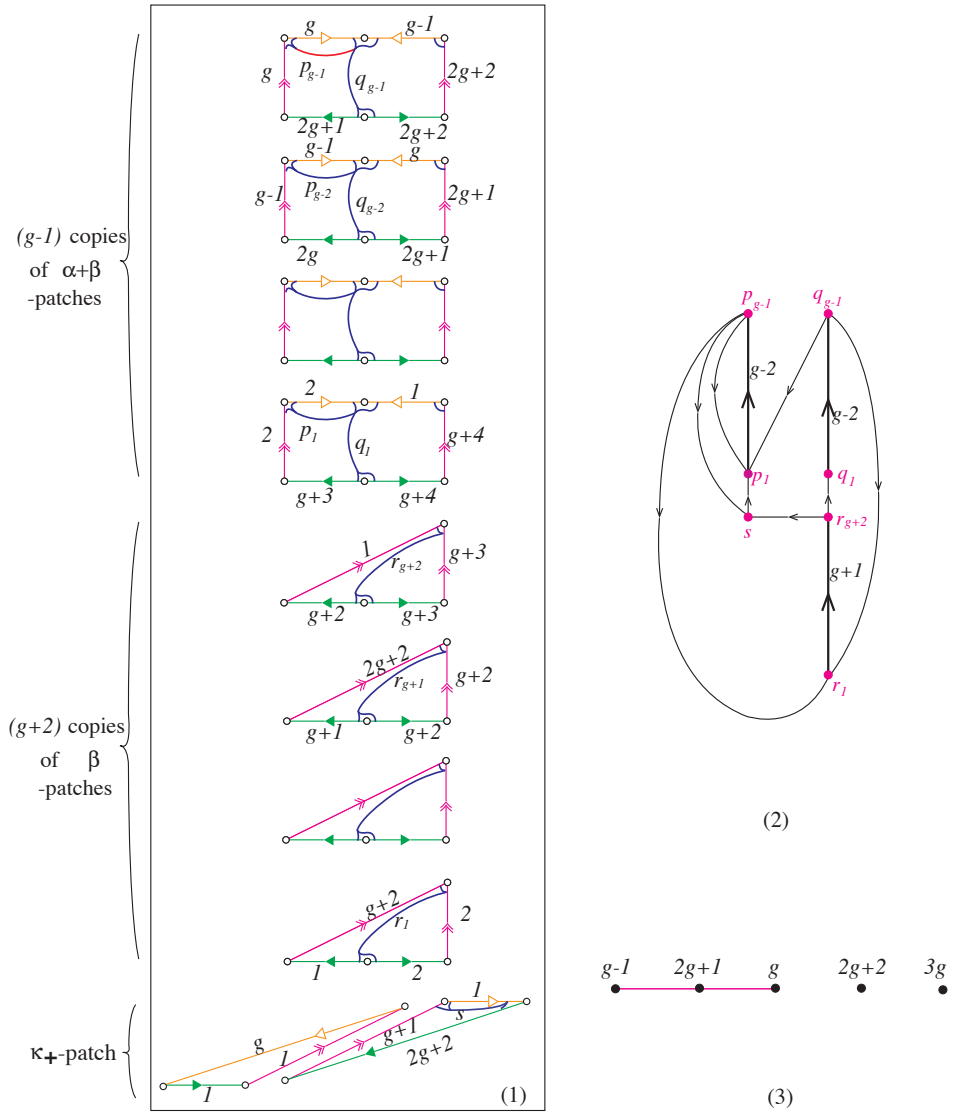

FIGURE 30. Example 4.2. (1) $\tau_{a_g} \subset F_{a_g}$ (2) Γ_{a_g} (3) G_{a_g} for $a_g = (1, g+2, g-1)_+$.

was found in [1] and [20] independently. However an explicit construction of a minimizer of δ_7^+ was not given in [1, 20]. Here we construct such a minimizer. Suppose that $g \equiv 7, 9 \pmod{10}$. Following [20], we take a sequence of primitive fibered classes

$$a_g = (g+6, 2, g)_+ = (2g+6, 2g+8, g+6) \in S_\beta(\tfrac{3}{-2}).$$

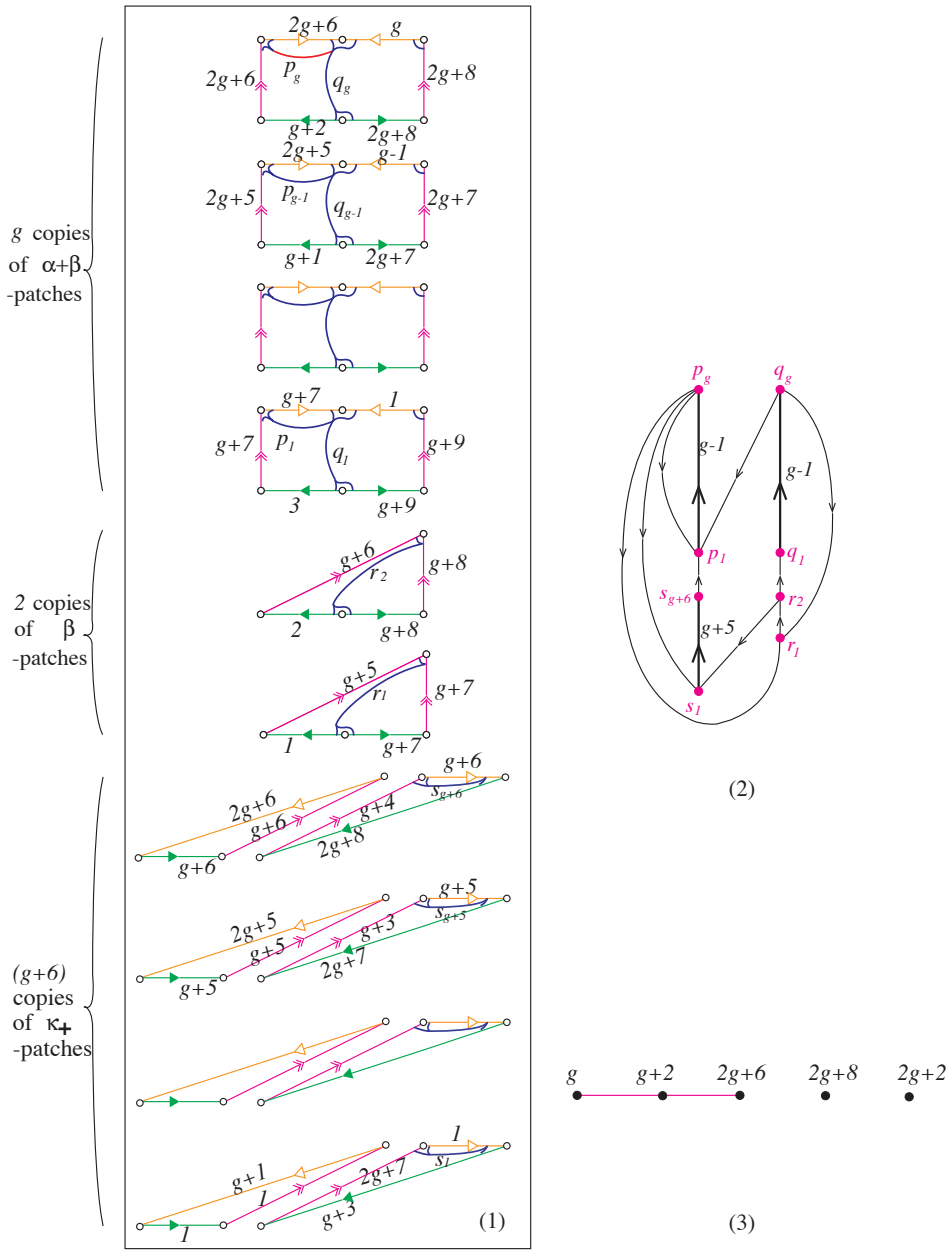

FIGURE 31. Example 4.3. (1) $\tau_{a_g} \subset F_{a_g}$ (2) Γ_{a_g} (3) G_{a_g} for $a_g = (g+6, 2, g)_+$.

Then F_{a_g} has genus g ([20]) and the projections $[a_g]$'s go to $[\frac{2}{3}, \frac{2}{3}] \in \mathrm{int}(\Delta)$ as g goes to ∞, see Figure 29(2). We have

$$Q_{(g+6,2,g)_+}(t) = (t^{g+4}+1)(t^{2g+4} - t^{g+4} - t^{g+2} - t^g + 1),$$

and the dilatation $\lambda_{(g+6,2,g)_+}$ is equal to the largest root of this polynomial. In particular $\lambda_{(g+6,2,g)_+}$ is equal to the largest root of the second factor of $Q_{(g+6,2,g)_+}(t)$. Lemma 2.6(7) ensures that the monodromy $\Phi_{a_g} : F_{a_g} \to F_{a_g}$ of the fibration associated to a_g extends to the pseudo-Anosov $\widehat{\Phi}_g : \Sigma_g \to \Sigma_g$ with orientable invariant foliations. It is known that δ_7^+ is equal to the largest root of the second factor of $Q_{(13,2,7)_+}(t)$ as above. Hence $\delta_7^+ = \lambda_{(13,2,7)_+}$, and the extension $\widehat{\Phi}_7$ of $\Phi_{(13,2,7)_+}$ is a minimizer of δ_7^+. The existence of the sequence of pseudo-Anosovs $\{\widehat{\Phi}_g\}$ was shown in [1, 20]. We have

$$\lim_{g\to\infty} g \log \lambda(\widehat{\Phi}_g) = \log(\tfrac{3+\sqrt{5}}{2}),$$

see the upper bounds (U1) and (U2).

Example 4.4 (Figure 32)**.** Suppose that $g \equiv 1, 5 \pmod{10}$. Following [20], we take a sequence of primitive fibered classes

$$a_g = (g+10, 4, g-2)_+ = (2g+8, 2g+12, g+10) \in S_\beta(\tfrac{3}{-2}).$$

Then the fiber F_g has genus g ([20]), and the dilatation $\lambda_{(g+10,4,g-2)_+}$ is equal to the largest root of

$$Q_{(g+10,4,g-2)_+}(t) = (t^{g+6}+1)(t^{2g+4} - t^{g+6} - t^{g+2} - t^{g-2} + 1).$$

Observe that the projections $[a_g]$'s go to $[\frac{2}{3}, \frac{2}{3}] \in \mathrm{int}(\Delta)$ as g goes to ∞, see Figure 29(2). We see that the monodromy $\Phi_{a_g} : F_{a_g} \to F_{a_g}$ of the fibration associated to a_g extends to the pseudo-Anosov $\widehat{\Phi}_g$ on Σ_g with orientable invariant foliations. The dilatation of $\widehat{\Phi}_g$ is the same as the dilatation of Φ_{a_g}, that is $\lambda_{(g+10,4,g-2)_+}$. The equality $\delta_5^+ = \lambda_{(15,4,3)_+}$ holds, see [21]. The sequence of pseudo-Anosovs $\{\widehat{\Phi}_g\}$ satisfies

$$\lim_{g\to\infty} g \log \lambda(\widehat{\Phi}_g) = \log(\tfrac{3+\sqrt{5}}{2}),$$

see the upper bounds (U1) and (U2).

Example 4.5 (Figure 33)**.** Following [17], we take a sequence of primitive fibered classes

$$a_n = (2n-1, 1, n-1)_- = (n-1, n, -2n+1) \in S_\gamma(1).$$

The dilatation $\lambda_{(2n-1,1,n-1)_-}$ is equal to the largest root of

$$Q_{(2n-1,1,n-1)_-}(t) = t^{4n-2} - t^{3n-1} - t^{3n-2} - t^n - t^{n-1} + 1.$$

The projections of a_n's go to $[\frac{1}{4}, \frac{1}{4}] \in \mathrm{int}(\Delta)$ as n goes to ∞, see Figure 29(3). We find that a_n defines a fibered class $\overline{a_n} \in H_2(N_\gamma(1), \partial N_\gamma(1))$, see the beginning of Section 4. By using Lemma 2.6(6), we see that the monodromy of the fibration on $N(1)$ associated to $\overline{a_n}$ has the dilatation $\lambda_{(2n-1,1,n-1)_-}$. Observe that the topological type of the fiber (i.e., minimal representative) of $\overline{a_n}$ is homeomorphic to $\Sigma_{1,2n-1}$. The sequence of the monodromies $\Phi_{\overline{a_n}}$

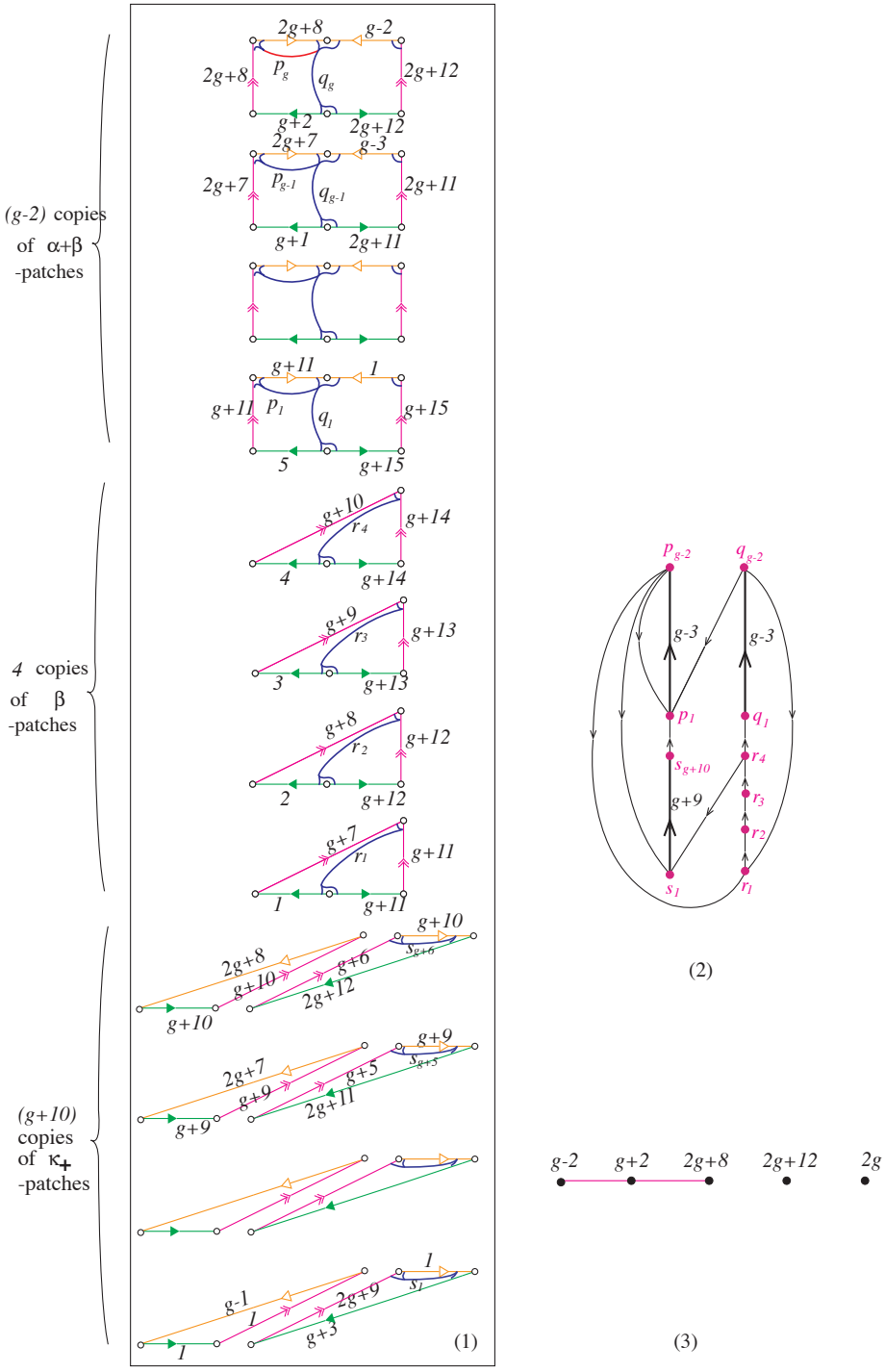

FIGURE 32. Example 4.4. (1) $\tau_{a_g} \subset F_{a_g}$ (2) Γ_{a_g} (3) G_{a_g} for $a_g = (g+10, 4, g-2)_+$.

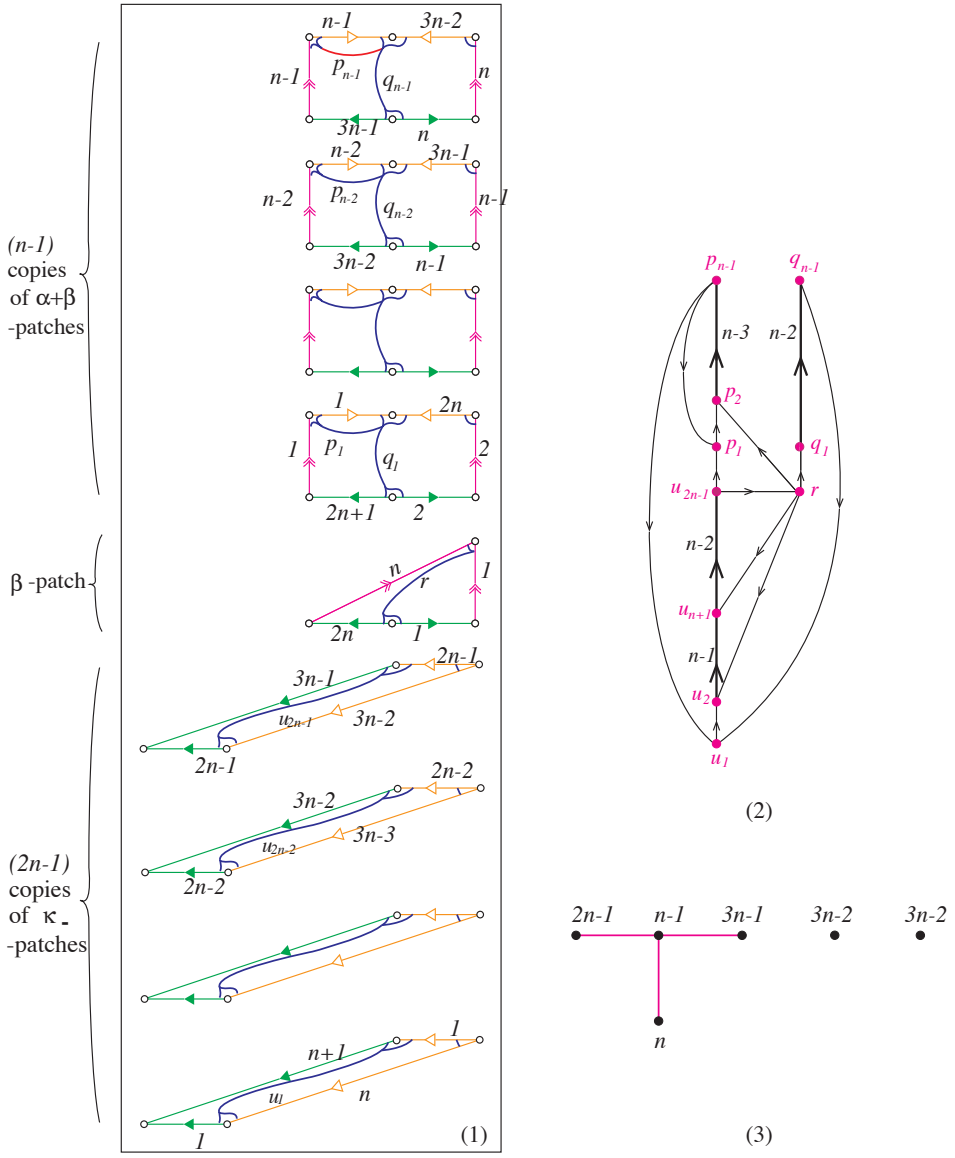

FIGURE 33. Example 4.5. (1) $\tau_{a_n} \subset F_{a_n}$ (2) Γ_{a_n} (3) G_{a_n} for $a_n = (2n-1, 1, n-1)_-$.

of fibrations associated to $\overline{a_n}$'s on the Whitehead link exterior $N_\gamma(1)$ can be used for a subsequence to prove (U5). In fact, we have

$$\lim_{n\to\infty} (2n-1) \log \lambda(\Phi_{\overline{a_n}}) = 2 \log \delta(D_4).$$

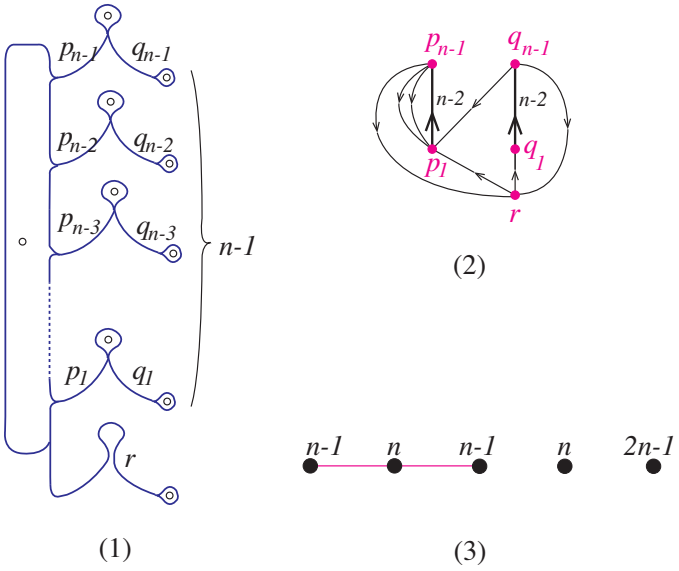

FIGURE 34. Example 4.6. (1) τ_{a_n} (circles indicate components of ∂F_{a_n}) (2) Γ_{a_n} (3) G_{a_n} for $a_n = (1, n-1)_0$.

Example 4.6 (Figure 34)**.** For $n \geq 3$, consider a sequence of primitive fibered classes

$$a_n = (1, n-1)_0 = (n-1, n, 0) \in S_\gamma(\infty),$$

which is studied in [18]. We see that F_{a_n} is homeomorphic to $\Sigma_{0,2n+1}$. The projection of a_n goes to $[\frac{1}{2}, \frac{1}{2}] \in \mathrm{int}(\Delta)$ as n goes to ∞, see Figure 29(4). The dilatation $\lambda_{(1,n-1)_0}$ equals the largest root of

$$Q_{(1,n-1)_0}(t) = t^{2n-1} - 2(t^{n-1} + t^n) + 1.$$

By using the same arguments as in Example 4.1(3), we see that the monodromy $\Phi_{a_n} : \Sigma_{0,2n+1} \to \Sigma_{0,2n+1}$ of the fibration associated to a_n defines the pseudo-Anosov $\overline{\Phi}_{a_n} : D_{2n-1} \to D_{2n-1}$ with the same dilatation $\lambda_{(1,n-1)_0}$. Such a pseudo-Anosov homeomorphism $\overline{\Phi}_{a_n} : D_{2n-1} \to D_{2n-1}$ is studied in [14]. It is known that $\delta(D_5) = \lambda_{(1,2)_0}$, see [9] and $\delta(D_7) = \lambda_{(1,3)_0}$, see [22]. The sequence of pseudo-Anosovs $\{\Phi_{a_n} : \Sigma_{0,2n-1} \to \Sigma_{0,2n-1}\}$ can be used for a subsequence to prove (U4):

$$\lim_{n\to\infty} (2n-1) \log \lambda(\Phi_{a_n}) = 2 \log(2 + \sqrt{3}).$$

Example 4.7 (Figure 35)**.** For $n \geq 2$, let us consider a sequence of fibered classes

$$a_n = (2, 2n-1)_0 = (2n-1, 2n+1, 0) \in S_\gamma(\infty),$$

which is studied in [18]. (The fibered class in Example 4.1(3) is equal to a_2 in the present example.) We see that F_{a_n} is homeomorphic to $\Sigma_{0,4n+2}$.

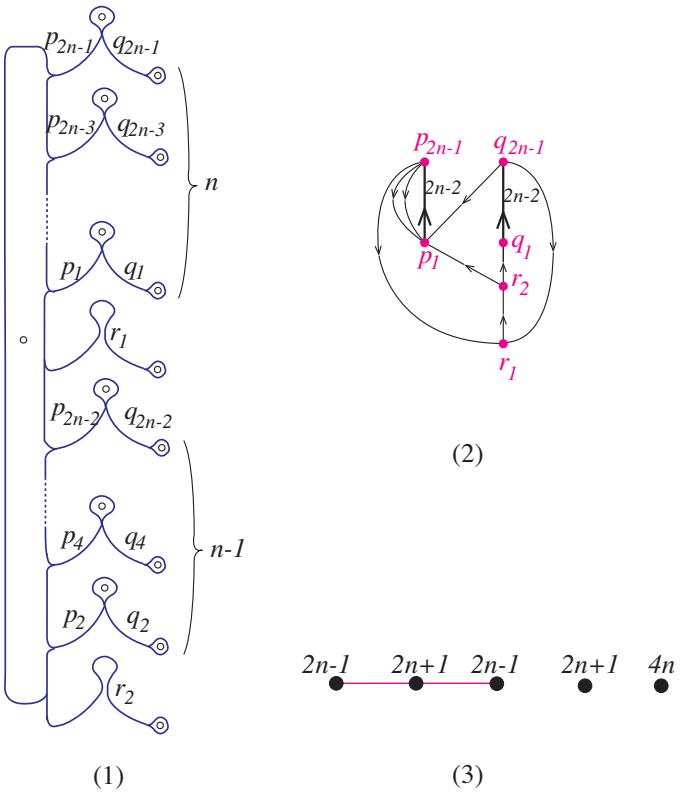

FIGURE 35. Example 4.7. (1) τ_{a_n} (2) Γ_{a_n} (3) G_{a_n} for $a_n = (2, 2n-1)_0$.

The projection of a_n goes to $[\frac{1}{2}, \frac{1}{2}] \in \mathrm{int}(\Delta)$ as n goes to ∞. The dilatation $\lambda_{(2,2n-1)_0}$ equals the largest root of

$$Q_{(2,2n-1)_0}(t) = t^{4n} - 2(t^{2n-1} + t^{2n+1}) + 1.$$

By using the same arguments as in Example 4.1(3), we see that the monodromy $\Phi_{a_n} : \Sigma_{0,4n+2} \to \Sigma_{0,4n+2}$ of the fibration associated to a_n defines the pseudo-Anosov $\overline{\Phi}_{a_n} : D_{4n} \to D_{4n}$ with the dilatation $\lambda_{(2,2n-1)_0}$. As we have seen in Example 4.1(3), the equality $\delta(D_8) = \lambda_{(2,3)_0}$ holds. Such a pseudo-Anosov homeomorphism $\overline{\Phi}_{a_n} : D_{4n} \to D_{4n}$ is also studied in [38]. The sequence of pseudo-Anosovs $\{\Phi_{a_n} : \Sigma_{0,4n+2} \to \Sigma_{0,4n+2}\}$ can be used for a subsequence to prove (U4):

$$\lim_{n\to\infty} (4n+2) \log \lambda(\Phi_{a_n}) = 2 \log(2 + \sqrt{3}).$$

Example 4.8 (Figure 36)**.** Throughout this example, we fix $g \geq 0$. The following sequence of fibered classes is used for the proof of Theorem 1.1,

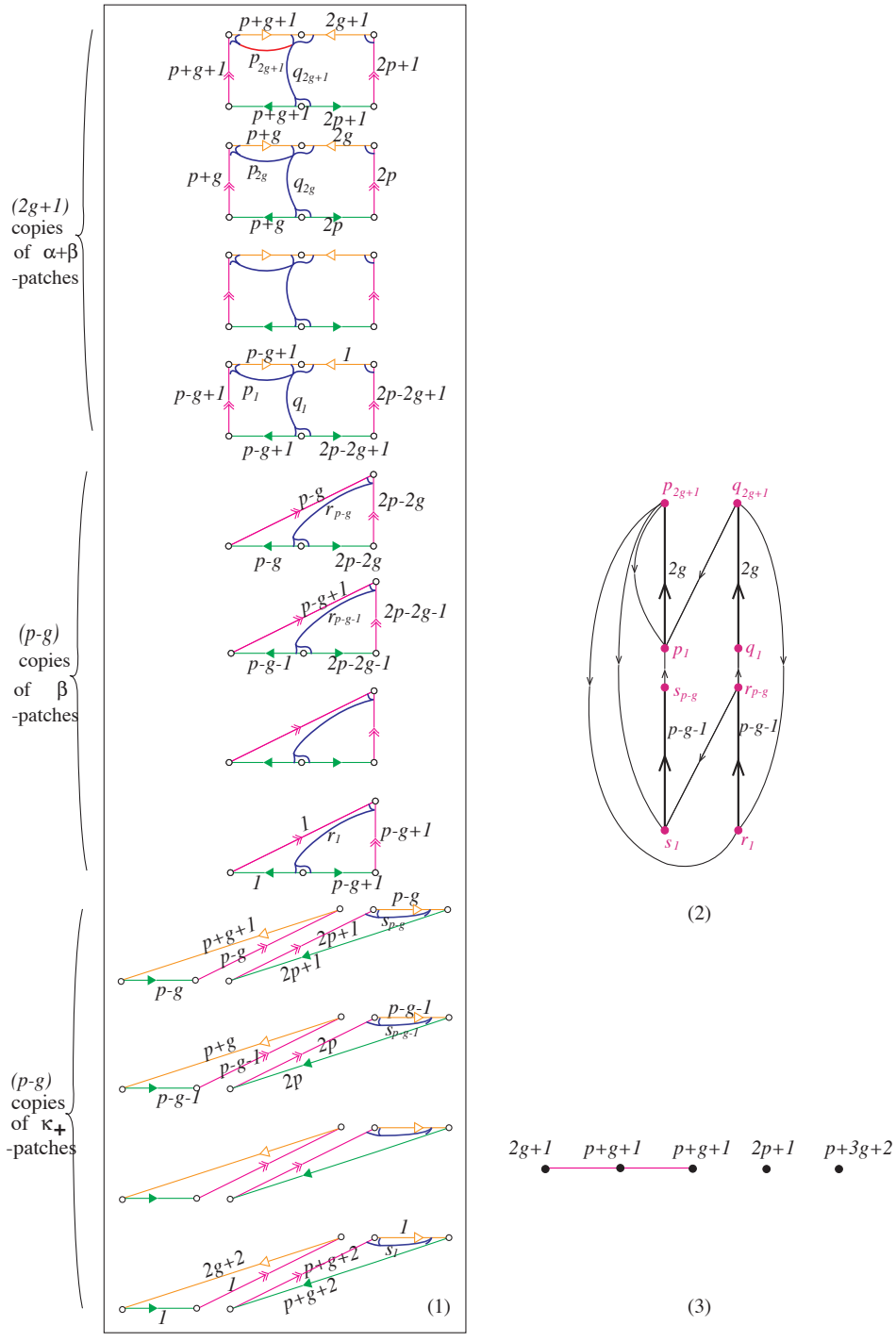

FIGURE 36. Example 4.8. (1) $\tau_{a_{(g,p)}} \subset F_{a_{(g,p)}}$ (2) $\Gamma_{a_{(g,p)}}$ (3) $G_{a_{(g,p)}}$ for $a_{(g,p)} = (p-g, p-g, 2g+1)_+$.

see [19]:

$$a_{(g,p)} = (p-g, p-g, 2g+1)_+ = (p+g+1, 2p+1, p-g) \in S_\beta(-1).$$

The projections $[a_{(g,p)}]$'s go to $[\frac{1}{2}, 1] \in \partial\Delta$ as p goes to ∞, see Figure 29(5). It is not hard to see that $a_{(g,p)}$ is primitive if and only if $2g+1$ and $p+g+1$ are relatively prime. If $a_{(g,p)}$ is primitive, then the fiber $F_{a_{(g,p)}}$ is homeomorphic to $\Sigma_{g,2p+4}$, and we have

$$\sharp(\partial_\beta F_{(g,p)}) = 2p+1 \text{ and } \sharp(\partial_\alpha F_{(g,p)}) + \sharp(\partial_\gamma F_{(g,p)}) = 3.$$

There exists a sequence of primitive fibered classes $\{a_{(g,p_i)}\}_{i=0}^{\infty}$ with $p_i \to \infty$ when $i \to \infty$, where p_i depends on g. (For example, take $p_i = (g+1)+i(2g+1)$.) This means that $F_{a_{(g,p_i)}}$ has genus g and the number of the boundary components of $F_{a_{(g,p_i)}}$ (which is equal to $2p_i+4$) goes to ∞ as i does. As we have seen above, the projection of such a class $a_{(g,p_i)}$ goes to the same point $[\frac{1}{2}, 1] \in \partial\Delta$ (which does not depend on g) as p_i goes to ∞.

References

[1] Aaber, John W.; Dunfield, Nathan. Closed surface bundles of least volume. *Algebr. Geom. Topol.* **10** (2010), no. 4, 2315–2342. MR2745673 (2012c:57030), Zbl 1205.57018, arXiv:1002.3423, doi: 10.2140/agt.2010.10.2315.

[2] Bestvina, M.; Handel, M. Train-tracks for surface homeomorphisms. *Topology* **34** (1995), no. 1, 109–140. MR1308491 (96d:57014), Zbl 0837.57010, doi: 10.1016/0040-9383(94)E0009-9.

[3] Birman, Joan S. PA mapping classes with minimum dilatation and Lanneau–Thiffeault polynomials. Preprint, 2011. arXiv:1104.2873.

[4] Cho, Jin-Hwan; Ham, Ji-Young. The minimal dilatation of a genus-two surface. *Experiment. Math.* **17** (2008), no. 3, 257–267. MR2455699 (2009i:37096), Zbl 1153.37375, doi: 10.1080/10586458.2008.10129045.

[5] Fathi, A.; Laudenbach, F.; Poenaru, V. Travaux de Thurston sur les surfaces. Séminaire Orsay. Astérisque, 66–67, *Société Mathématique de France, Paris*, 1979. MR568308 (82m:57003), Zbl 0406.00016.

[6] Fried, David. Fibrations over S^1 with pseudo-Anosov monodromy. Exposé 14 in 'Travaux de Thurston sur les surfaces'. *Astérisque* **66–67** (1979), 251–266. Zbl 0446.57023.

[7] Fried, David. Flow equivalence, hyperbolic systems and a new zeta function for flows. *Comment. Math. Helv.* **57** (1982), no. 2, 237–259. MR0684116 (84g:58083), Zbl 0503.58026, doi: 10.1007/BF02565860.

[8] Gantmacher, F.R. The theory of matrices. Vol. 2. Translated by K. A. Hirsch. Reprint of the 1959 translation. *Chelsea Publishing Co., New York* 2000. ix+276 pp. MR107649 (21 #6372c), Zbl 0927.15002.

[9] Ham, Ji-Young; Song, Won Taek. The minimum dilatation of pseudo-Anosov 5-braids. *Experiment. Math.* **16** (2007), no. 2, 167–179. MR2339273 (2008e:37043), Zbl 1151.37037, arXiv:math/0506295, doi: 10.1080/10586458.2007.10129000.

[10] Hironaka, Eriko. Small dilatation mapping classes coming from the simplest hyperbolic braid. *Algebr. Geom. Topol.* **10** (2010), no. 4, 2041–2060. MR2728483 (2012e:57033), Zbl 1221.57028, doi: 10.2140/agt.2010.10.2041.

[11] Hironaka, Eriko. Mapping classes associated to mixed-sign Coxeter graphs. Preprint, 2011. arXiv:1110.1013.

[12] Hironaka, Eriko. Quotient families of mapping classes. Preprint, 2012. arXiv:1212.3197.

[13] Hironaka, Eriko. Small dilatation pseudo-Anosov mapping classes and short circuits on train track automata. Mittag-Leffler Institute Preprint Collection, Workshop on Growth and Mahler Measures in Geometry and Topology, (Djursholm, Sweden) (2014), 17–41. arXiv:1403.2987.

[14] Hironaka, Eriko; Kin, Eiko. A family of pseudo-Anosov braids with small dilatation. *Algebr. Geom. Topol.* **6** (2006), 699–738. MR2240913 (2008h:57027), Zbl 1126.37014, arXiv:math/0507012, doi: 10.2140/agt.2006.6.699.

[15] Ivanov, N.V. Coefficients of expansion of pseudo-Anosov homeomorphisms. *Zap. Nauchn. Sem. Leningrad. Otdel. Mat. Inst. Steklov. (LOMI)* **167** (1988), Issled. Topol. 6, 111–116, 191; *translation in J. Soviet Math.* **52** (1990), no. 1, 2819–2822. MR0964259 (89i:32047), Zbl 0707.57007, doi: 10.1007/BF01099245.

[16] Kin, Eiko. Notes on pseudo-Anosovs with small dilatations coming from the magic 3-manifold. Representation spaces, twisted topological invariants and geometric structures of 3-manifolds. *RIMS Kokyuroku* **1836** (2013), 45–64. `http://www.math.sci.osaka-u.ac.jp/~kin/publication/note_hakone.pdf`.

[17] Kin, Eiko; Kojima, Sadayoshi; Takasawa, Mitsuhiko. Minimal dilatations of pseudo-Anosovs generated by the magic 3-manifold and their asymptotic behavior. *Algebr. Geom. Topo.* **13** (2013), no. 6, 3537–3602. MR3248741, Zbl 1306.37042, arXiv:1104.3939, doi: 10.2140/agt.2013.13.3537.

[18] Kin, Eiko; Takasawa, Mitsuhiko. Pseudo-Anosov braids with small entropy and the magic 3-manifold. *Comm. Anal. Geom.* **19** (2011), no. 4, 705–758. MR2880213, Zbl 1251.37047, arXiv:0812.4589, doi: 10.4310/CAG.2011.v19.n4.a3.

[19] Kin, Eiko; Takasawa, Mitsuhiko. The boundary of a fibered face of the magic 3-manifold and the asymptotic behavior of the minimal pseudo-Anosovs dilatations. Preprint, 2012. arXiv:1205.2956.

[20] Kin, Eiko; Takasawa, Mitsuhiko. Pseudo-Anosovs on closed surfaces having small entropy and the Whitehead sister link exterior. *J. Math. Soc. Japan* **65** (2013), no. 2, 411–446. MR3055592, Zbl 1270.57044, arXiv:1003.0545, doi: 10.2969/jmsj/06520411.

[21] Lanneau, Erwan; Thiffeault, Jean-Luc. On the minimum dilatation of pseudo-Anosov homeomorphisms on surfaces of small genus. *Ann. Inst. Fourier* **61** (2011), no. 1, 105–144. MR2828128 (2012e:37070), Zbl 1237.37027, arXiv:0905.1302, doi: 10.5802/aif.2599.

[22] Lanneau, Erwan; Thiffeault, Jean-Luc. On the minimum dilatation of braids on punctured discs. *Geom. Dedicata* **152** (2011), 165–182. MR2795241 (2012h:57035), Zbl 1230.37047, arXiv:1004.5344, doi: 10.1007/s10711-010-9551-2.

[23] Long, Darren D.; Oertel, Ulrich. Hyperbolic surface bundles over the circle. *Progress in knot theory and related topics*, 121–142, Travaux en Cours, 56. *Hermann, Paris*, 1997. MR1603150 (98m:57022), Zbl 0959.57019.

[24] Los, Jérôme. Infinite sequence of fixed-point free pseudo-Anosov homeomorphisms. *Ergodic Theory Dynam. Systems* **30** (2010), no. 6, 1739–1755. MR2736893 (2012h:37087), Zbl 1213.37071, arXiv:0806.4027, doi: 10.1017/S0143385709000832.

[25] Martelli, Bruno; Petronio, Carlo. Dehn filling of the "magic" 3-manifold. *Comm. Anal. Geom.* **14** (2006), no. 5, 969–1026. MR2287152 (2007k:57042), Zbl 1118.57018, arXiv:math/0204228, doi: 10.4310/CAG.2006.v14.n5.a6.

[26] Matsumoto, Shigenori. Topological entropy and Thurston's norm of atoroidal surface bundles over the circle. *J. Fac. Sci. Univ. Tokyo Sect. IA Math.* **34** (1987), no. 3, 763–778. MR0927609 (89c:57011), Zbl 0647.57006.

[27] McMullen, Curtis T. Polynomial invariants for fibered 3-manifolds and Teichmüler geodesics for foliations. *Ann. Sci. École Norm. Sup.* (4) **33** (2000), no. 4, 519–560. MR1832823 (2002d:57015), Zbl 1013.57010, doi: 10.1016/S0012-9593(00)00121-X.

[28] McMullen, Curtis T. Entropy and the clique polynomial. *J. Topol.* **8** (2015), no. 1, 184–212. MR3335252, Zbl pre06417724, doi: 10.1112/jtopol/jtu022.

[29] Minakawa, Hiroyuki. Examples of pseudo-Anosov homeomorphisms with small dilatations. *J. Math. Sci. Univ. Tokyo* **13** (2006), no. 2, 95–111. MR2277516 (2007m:37073), Zbl 1119.37024.

[30] Oertel, Ulrich. Homology branched surfaces: Thurston's norm on $H_2(M^3)$. *Low-dimensional topology and Kleinian groups* (Coventry/Durham, 1984), 253–272, London Math. Soc. Lecture Note Ser., 112. *Cambridge Univ. Press, Cambridge*, 1986. MR0903869 (89e:57011), Zbl 0628.57011.

[31] Oertel, Ulrich. Affine laminations and their stretch factors. *Pacific J. Math.* **182** (1998), no. 2, 303–328. MR1609595 (99i:57037), Zbl 0909.57008, doi: 10.2140/pjm.1998.182.303.

[32] Papadopoulos, Athanase; Penner, Robert C. A characterization of pseudo-Anosov foliations. *Pacific J. Math.* **130** (1987), no. 2, 359–377. MR0914107 (88k:57015), Zbl 0602.57019, doi: 10.2140/pjm.1987.130.359.

[33] Penner, R. C. Bounds on least dilatations. *Proc. Amer. Math. Soc.* **113** (1991), no. 2, 443–450. MR1068128 (91m:57010), Zbl 0726.57013, doi: 10.2307/2048530.

[34] Song, Won Taek; Ko, Ki Hyoung; Los, Jérôme E. Entropies of braids. *J. Knot Theory Ramifications* **11** (2002), no. 4, 647–666. MR1915500 (2003e:57013), Zbl 1010.57004, doi: 10.1142/S021821650200186X.

[35] Thurston, William P. A norm for the homology of 3-manifolds. *Mem. Amer. Math. Soc.* **59** (1986), no. 339, i –vi and 99–130. MR0823443 (88h:57014), Zbl 0585.57006.

[36] Thurston, William P. Hyperbolic structures on 3-manifolds II: Surface groups and 3-manifolds which fiber over the circle. Preprint, 1998. arXiv:math/9801045.

[37] Tsai, Chia-Yen. The asymptotic behavior of least pseudo-Anosov dilatations. *Geom. Topol.* **13** (2009), no. 4, 2253–2278. MR2507119 (2010d:37081), Zbl 1204.37043, arXiv:0810.0261, doi: 10.2140/gt.2009.13.2253.

[38] Venzke, R. Braid forcing, hyperbolic geometry, and pseudo-Anosov sequences of low entropy. PhD thesis, California Institute of Technology, 2008. `http://thesis.library.caltech.edu/2253/`.

[39] Zhirov, A. Yu. On the minimum dilation of pseudo-Anosov diffeomorphisms on a double torus. *Russian Math. Surveys* **50** (1995), no. 1, 223–224. MR1331364 (96e:58123), Zbl 0847.58057, doi: 10.1070/RM1995v050n01ABEH001680.

(Eiko Kin) Department of Mathematics, Graduate School of Science, Osaka University Toyonaka, Osaka 560-0043, JAPAN
`kin@math.sci.osaka-u.ac.jp`

This paper is available via `http://nyjm.albany.edu/j/2015/21-25.html`.